2012

Elements of Deformation and Stretching in Vertebrate Bodies

Matthew Thomas Close
Lehigh University

Elements of Deformation and Stretching in Vertebrate Bodies

by

Matthew Thomas Close

A Dissertation

Presented to the Graduate and Research Committee

of Lehigh University

in Candidacy for the Degree of

Doctor of Philosophy

in

Integrative Biology

Lehigh University

September 2012

Approved and recommended for acceptance as a dissertation in partial fulfillment of the requirements for the degree of Doctor of Philosophy

Matthew Thomas Close
Elements of Deformation and Stretching in Vertebrate Bodies

July 13, 2012
Defense Date

David Cundall
Dissertation Director

July 27, 2012
Approved Date

Committee Members:

Lynne Cassimeris

Matthias Falk

Nathan Kley

Alan Savitzky

ACKNOWLEDGEMENTS

David Cundall spent many years training me to be a scientist and a teacher. He provided me with an environment of intellectual freedom, and though I freely made numerous mistakes through the years, his training, advice and criticism were crucial to my professional development. I began graduate school completely unprepared for academic life, and I am now fully engaging it largely because of his investment in me.

Lynne Cassimeris served on my dissertation committee and freely offered advice on all things cellular. She also fostered a healthy collaboration with my colleagues at the University of Pennsylvania. Dr. Matthias Falk served on my dissertation committee with short notice, and also allowed me to conduct some of my preliminary research in his lab. Some of the members of his lab group, Tia Kowal, Rachael Kells and Sarah Mollerup, offered their technical assistance along the way.

Clara Franzini-Armstrong of the University of Pennsylvania provided both her expertise and her laboratory to carry out parts of my dissertation research. Stefano Perni of the University of Pennsylvania was directly involved with my research. Without his time and effort I could not have answered many of the questions that interested me, and the dissertation would have taken a different direction.

Nathan Kley of Stonybrook University served on my dissertation committee and offered advice throughout the dissertation writing process. His extensive knowledge of functional morphology and his very careful eye were crucial to planning, carrying out and writing up my research.

Alan Savitzky of Utah State University was involved in virtually every step of my professional development. While at Old Dominion University, Al planted a seed in an

undergraduate that eventually matured into the Ph.D. candidate who wrote this dissertation. He encouraged me to work my first herpetological job as a field research technician and then later encouraged me to pursue a graduate career in herpetology. He later agreed to serve on my dissertation committee even though he had numerous other personal and professional obligations. I thank Al for sharing his enthusiasm for herpetological research, for freely offering his advice, and for sacrificing his time to ensure that I succeeded.

Lehigh University's College of Arts and Sciences, Sigma Xi Scientific Research Society and the Herpetologists' League provided funding for my research projects. The Graduate Student Senate and the Department of Biological Sciences at Lehigh University both provided travel support for meetings I attended.

Several interdepartmental colleagues at Lehigh University helped me with practical aspects of my research. Bruce Hargreaves, Bruce Idleman and Joseph Seem of the Department of Earth and Environmental Sciences offered access to equipment and provided valuable instruction. I give a special thanks to Joe for offering his time and assistance with building research equipment. Richard Vinci and Walter Brown of Materials Science and Engineering provided access to equipment and instructed a biologist in all things mechanical. I give special thanks to Walter for helping me design and build mechanical testing equipment. Joseph Constantino assisted in carrying out preliminary experiments for some of my dissertation research.

Much of what I learned through graduate school was learned because I was challenged to communicate information clearly to a broad but scientifically literate

audience for 14 semesters. My students shared their enthusiasm for science with me and encouraged me to excel as both a scholar as well as a teacher.

My family and friends have been a source of emotional and financial support. My mother, Carolyn Close and father, Truman Close, Jr., invested tremendous amounts of time and resources throughout my life and challenged me to strive for the best. My siblings, Gregory Close, Julie Parker and John Close, provided much encouragement and practical guidance. Charles and Katherine Grau offered a tremendous amount of financial and emotional support, and are incredible in-laws.

My wife, Emily Close, stood beside me every day, had faith when I had none, and made numerous sacrifices to see me through graduate school. My daughters, Olivia and Clara, sacrificed time with me to allow me to return to the lab to conduct research and/or write. My girls have certainly made life interesting, and though they presented challenges they have been a source of joy for me through these years. Finally, I thank God for all he has done to make this possible. In my pursuit of knowledge, he is often forgotten, ignored and even doubted, but he has ultimately been my source of hope through these years.

TABLE OF CONTENTS

LIST OF FIGURES

LIST OF TABLES

ABSTRACT

I conducted a study of dynamic aspects of predator and prey morphology in the feeding system of snakes. The objectives were to 1) understand better the ingestible size of rodents, a common prey of many snakes, and 2) determine the changes occurring in soft tissues of the lower jaw of snakes under conditions similar to intraoral prey transport.

I examined the deformability of rodents by comparing cross-sectional areas of 100 rodents (50 *Mus musculus* and 50 *Rattus norvegicus*) across four treatments and scaled mass and linear measures of rodents to smallest-attainable cross-sectional area obtained from manipulations. Rolling prey into cylinders significantly reduced prey cross-sectional area, and radiographic images revealed that this occurred by musculoskeletal changes similar to those seen following ingestion by a snake. Linear measures of prey at rest overestimated ingestible size, but mass underestimated it.

During intraoral transport, the distance between the mandibular rami of Northern watersnakes (*Nerodia sipdeon*) increases more than 700% resting distance, and I examined the effect of lower jaw distension on the intermandibular soft tissues. First, I compared the histology of skin in resting, moderately stretched and highly stretched conditions. Moderate extension unfolds interscale skin regions, reorganizing the extracellular matrix of the dermis. Increased extension flattens interscale skin by stretching the interscale dermis and epidermis. Elastin fibers are abundant in the dermis and I suggest a mechanism by which they restore interscale skin to its folded resting state.

Second, I compared the ultrastructure of resting, stretched, and recovered conditions of a lower jaw muscle (*Musculus intermandibularis anterior, pars anterior*)

using transmission electron microscopy. Sarcomere lengths from stretched fibers were 210% those of resting fibers, and concomitant changes included non-overlapping myofilaments, misalignment of triads and cytoskeletal elements, and misalignment of Z-lines from adjacent myofibrils. Sarcomere lengths from recovered fibers were 82% those of resting fibers resulting in double-overlap of actin at mid-sarcomere and realignment of triads and Z-lines. Discrepancy between extension of whole muscle (270%) and sarcomeres (210%) results from folded tendon fibrils and abundant epimyseal elastin. Highly extended muscle returns to its resting condition primarily by exploiting intra- and extracellular passive elastic elements.

CHAPTER 1

General Introduction

The research described in this dissertation was conducted to answer two main questions: 1) how do rodent prey change when they are swallowed by snakes? and 2) how do the intermandibular soft tissues of snakes change under high levels of extension, as seen when they swallow relatively large prey. The first question is addressed in Chapter Two, in which I define ingestible size of rodents, describe how it can be measured and relate this measure to measurements of body size and to dynamic changes in anatomical form. The second question is answered in two parts. In Chapter Three, I describe and quantify the anatomical and histological changes occurring in skin that accompany varying levels of lower jaw extension, and I provide a model for how skin reaches high levels of strain and subsequently returns to its resting condition. In Chapter Four, I describe and quantify the histological and ultrastructural changes that accompany high levels of extension of a snake lower jaw muscle and its subsequent return to rest.

Chapter Two details a morphological study of the deformation of mammal bodies whereas Chapters Three and Four describe the functional morphology of two highly extensible soft tissues in snakes—skin and muscle. The three projects differ in terms of taxa used, methodology and scale, but they are conceptually related. Snakes swallow their prey whole, and therefore their ability to ingest prey depends on 1) the ability of the feeding apparatus to passively conform (i.e., stretch) to prey size (Cundall and Greene, 2000) and 2) the ability of prey size to conform passively to loads applied by the snake's feeding apparatus.

Mammals are the prey of many snake species (Greene, 1997) and because their bodies lack a rigid integument or a highly muscular trunk, they are moderately deformable. Studies of prey size/ predator size relationships in snakes that eat mammals have measured prey size based on linear measures of prey and prey mass (Arnold, 1993; Forsman and Lindell, 1993; Glaudas et al., 2008; Mori, 1991; Rodríguez-Robles, 2002; Rodríguez-Robles et al., 1999a,b) but these measures alone are problematic to use as prey size measures because 1) linear measures of rodents are changeable (Dobson, 1992; Iskjaer et al., 1989; Jewell and Fullagar, 1966) and 2) mass, by itself, relays little information about linear or area measures. Therefore, in Chapter Two I studied two species of murids commonly used in laboratory feeding experiments (*Mus musculus* and *Rattus norvegicus*) to test the hypothesis that prey size (which, in the context of snake feeding, is cross-sectional area) is changeable and that the ingestible size of a rodent is smaller than a measure of the same rodent at rest. I then describe the linear relationships between standard measures of prey and my new measure of prey size (ingestible size), and describe the anatomical changes that accompany the deformation associated with changing a rodent's size.

Chapters Three and Four focus on two projects aimed at addressing a major gap in snake feeding literature: understanding the extensibility of the soft tissues linking the tips of the mandibles (Arnold, 1983; Cundall and Greene, 2000). Though many of the details of the connection of the mandibles in snakes have been described previously (Cundall, 1995; Groombridge, 1979; Haas, 1973; Kiran, 1981; Langebartel, 1968; Young, 1998a,b), virtually nothing is known about what actually occurs (at anatomical or histological levels) in these tissues when stretched. This problem was formally pointed

out more than a decade ago (Cundall and Greene, 2000), and I attempted to address this by detailing changes that occur in two of the soft tissues (skin and muscle) under levels of extension seen in snakes when they feed. I collected over 1000 behavioral records from eight species of snakes feeding in the lab to formulate my hypotheses about how the intermandibular soft tissues behave. For the behavioral, anatomical and histological data presented in this dissertation, I used Northern watersnakes (*Nerodia sipedon*) because they were easy to collect in the field from nearby urban populations and because neonates could be obtained easily. This enabled me to investigate morphology at multiple scales using larger sample sizes.

Chapter Three has two main objectives: First, it details the findings of my behavioral records of snakes feeding on relatively large prey in the laboratory and the mechanical testing of snake lower jaws *in vivo*. These data were used to determine appropriate levels of extension to apply for experimental manipulations. Second, it details a study on the functional morphology of snake skin. The integument is one of many morphological characters that distinguish vertebrate taxa from one another (Brusca and Brusca, 2003; Kardong, 2012), and though it always forms the barrier to the external environment, specializations often confer vast functional differences. These specializations occur both between and within species, but can also vary within an individual organism. The anterior half of macrostomatan snakes is highly modified for the ingestion of relatively large prey (Gans, 1961; Cundall and Greene, 2000; Rivera et al., 2004), and I therefore determine how skin in the most extensible portion of the snake responded to high levels of extension seen during feeding. Specifically, I test the hypothesis that the resting, moderately stretched and highly stretched conditions differ in

terms of their anatomical and histological arrangement. I then use the information gathered to arrive at a general model for how skin is passively reorganized following an extreme level of extension.

Chapter Four details the findings of a histological and ultrastructural study on the extensibility of a snake lower jaw muscle, the *musculus intermandibularis anterior pars anterior* (MIAA). This study was conducted in collaboration with the laboratory of Clara Franzini-Armstrong at the University of Pennsylvania.

The structural basis of passive extensibility of vertebrate skeletal muscle contains at least two components: elasticity of cells and elasticity of the extracelllular matrix (Wang et al., 1993). The former rests on cell membrane properties (Dulhunty and Franzini-Armstrong, 1975) as well as intracellular elastic proteins (Horowitz et al. 1986; Pierobon-Bormioli, 1981; Salviati et al. 1990; Wang et al., 1983; Wang et al. 1993), whereas the latter rests on relationships between cells and the extracellular matrix, cross-linking between proteins of the extracellular matrix, and elasticity of proteins of the extracellular matrix (Borg and Caulfield, 1980; Purslow, 1989; Rowe, 1981). In Chapter Four, I test the hypothesis that the cytoskeleton of the *musculus intermandibularis anterior pars anterior* (MIAA) undergoes major deformations during levels of extension, but that these deformations are passively recoverable. I use ultrastructural data gathered by transmission electron microscopy to investigate these details because they were not resolvable using light or fluorescence microscopy. I also explain extensibility of muscle in terms of its histological organization, and therefore describe 1) how cells responded to stretch in terms of their relationship to adjacent cells and 2) the mechanism for whole-muscle recovery.

CHAPTER 2

Estimating Prey Size

INTRODUCTION

Accurate, repeatable measures of animals that lack either a rigid integument or rigid musculoskeletal bauplan, such as mammals, are difficult to obtain (Jewell and Fullagar, 1966). Studies of mammalian life history traits have long been plagued by the problem of body size, and these problems are most evident when trying to scale linear dimensions to mass (Silva, 1998). Iskjaer et al. (1989) stated that body size in mammals was a "nebulous quantity to measure," and suggested a multivariate approach to the problem of measuring size in relation to mammalian life history traits. Dobson (1992) pointed out that rates of change in mass are really functions of both structural size, defined as the size of the supporting tissues, and physiological condition, which is dependent on the size of energy reserves. In each case mass is of limited value to studies using structural size comparisons because the factors that either contribute to or result from changes in mass are labile. While the difficulty of measuring deformable body forms is rather obvious, it is easily overlooked in much of the ecological literature.

Vezina (1985) demonstrated that among predatory animals, the prey-to-predator mass ratio is highest among carnivores when compared to piscivores and insectivores. Prey size is extremely important to carnivores that ingest their food whole. For snakes, the predator's maximal gape determines the size of the largest prey that can be consumed (Greene, 1983), and the critical feature of mammal prey is the smallest attainable cross-sectional area of the largest part of the body (Arnold, 1983; Cundall and Greene, 2000).

The problem then, for both snakes and biologists interested in measuring mammals eaten by snakes, is estimating that variable.

Arnold (1993) reviewed much of the existing literature on predator and prey size relationships in snakes. Prey size was typically extracted from one or several measurements including mass, length (snout-vent length, total body length, or standard length), width (or diameter), and/or volume. The condition of material available determined sample sizes and the measures used. Most studies relied on measurements of intact prey, a rare occurrence in predator stomach or fecal contents. When prey species in stomach or fecal contents could be identified, measures of prey size were sometimes gained from conspecific museum specimens. Recent studies incorporate average conspecific prey mass, length and width/diameter (Glaudas et al., 2008; Rodríguez-Robles, 2002; Rodríguez-Robles et al., 1999a,b) to arrive at prey size estimates, but the relationships among all measures of size used are rarely reported. Mass is the most widely used measure of the size of mammals used in the laboratory studies of snake feeding behavior (Forsman and Lindell, 1993; Mori, 1991), but prey height, width (diameter) and length (measured as either snout to anus length or head and body length) have been used to test the correlations with a particular measure of feeding performance (Mori, 1991; Pough and Groves, 1983; Shine, 1991). Predator-prey mass ratios (Greene, 1983; Pough and Groves, 1983; Kley and Brainerd, 2002; Mehta, 2009) and ingestion ratios (Greene, 1983), such as prey caliber to head caliber (Loop and Bailey, 1972), prey mass to head length (Shine, 1991) or prey height to lower jaw length (Cundall and Deufel, 2006), have been used less frequently.

Researchers interested in studying gape-limited predators that feed on mammals are thus faced with the following problems: The relative size of prey influences predator performance, but the linear dimensions, and thus absolute size, of mammals are changeable. Mass is an unchanging measure of a body's absolute size, but alone it provides little information on linear dimensions of elastic body simply because a single change in one dimension will result in a change in at least one other dimension. Therefore, we test the relationship between a mammal's mass, linear dimensions and ingestible size, defined as the smallest attainable cross-sectional area of the largest part of the body. In order to determine the effect of deformability on estimated cross-sectional area, we first explore differences among cross-sectional area estimates of freshly killed rodents derived from four different measurement protocols. Specifically, we test the hypothesis that measures of freshly killed, resting rodents give estimates of cross-sectional area higher than measures of the same rodents rolled tightly into cylinders. We then ask which musculoskeletal features change when rodents are rolled into cylinders and whether this deformation approximates what occurs when a snake swallows a rodent. Finally, we determine the scaling relationships between measures of mass, length, height and width of unmanipulated rodents and the smallest attainable cross-sectional area in order to generate a method of estimating rodent ingestible size from single mass or linear measurements alone.

METHODS

To estimate relationships between cross-sectional area and other measures of rodents, MTC measured 50 juvenile to adult Norway rats (*Rattus norvegicus*) and 50

juvenile to adult house mice (*Mus musculus*) of both sexes. Because pregnancy causes significant changes in the body form of female rodents, no conspicuously gravid females were used (Dewsbury, 1992). All rodents were reared and housed in the laboratory under normal light and temperature conditions with *ad libitum* access to food and water. All animals were humanely sacrificed prior to measuring using CO_2 anesthesia to cessation of heartbeat. Methods were approved under Lehigh University IACUC protocol 66.

Cross-sectional Area Estimates

Cross-sectional area was estimated for each rodent from four different manipulations (see below). For three manipulations, cross-sectional area (A) was derived as the area of an ellipse using the following equation:

$$A = \frac{\pi ab}{4}$$

where major (*a*) and minor (*b*) axes were derived from height and width measurements described below. For the fourth manipulation, cross-sectional area was derived as the area of a cylinder of a given length (*L*) and fixed volume (*V)* using the following equation:

$$A = \frac{V}{L}$$

All linear measurements were taken to the nearest 0.1mm using dial calipers. Measurements of mass were made to the nearest 0.1g.

Height Width (HW) method: Height and width of rodents were taken at approximately the highest and widest points of the prey following Cundall and Deufel (2006) for height and

Pough and Groves (1983) for width. For all specimens we measured, the widest point occurred at the level of the pelvic girdle (Fig. 1A) and the highest point lay at the middle of the trunk (Fig. 1B).

Rolled (Ro) method: To test the effect of uniform pressure along the entire length of a rodent body on cross-sectional area, as possibly experienced by rodents following complete engulfment, rodents were rolled tightly into cylinders using pieces of 70lb. paper cardstock (Fig. 1C,D). Prey height and width (usually the same) were measured from the inner height and width of the paper cylinder.

Wrapped (Wr) method: Rodents were tightly wrapped from the snout to the pelvic girdle using surgical gauze (Fig. 1E,F). This procedure simulates the effect snakes have on prey form during ingestion, shifting much of the visceral volume caudally and enlarging the caudal end relative to the head and trunk (Fig. 2). Height and width of the caudal end of the prey were measured at the level of the pelvic girdle just past the end of the gauze (Fig. 1E,F).

Volumetric (Vo) method: Assuming that rodent bodies could be viewed as cylindrical masses, we derived cross-sectional area using rodent length and the volume of the head and trunk. Length was measured as the distance from the tip of the snout to the base of the tail using calipers for mice and small rats and a ruler for large rats. Rodents were laid on their backs to reduce the effects of the curvature of the spine (Jewell and Fullagar, 1966). Rodent head and body volume was measured to the nearest 1ml by volumetric

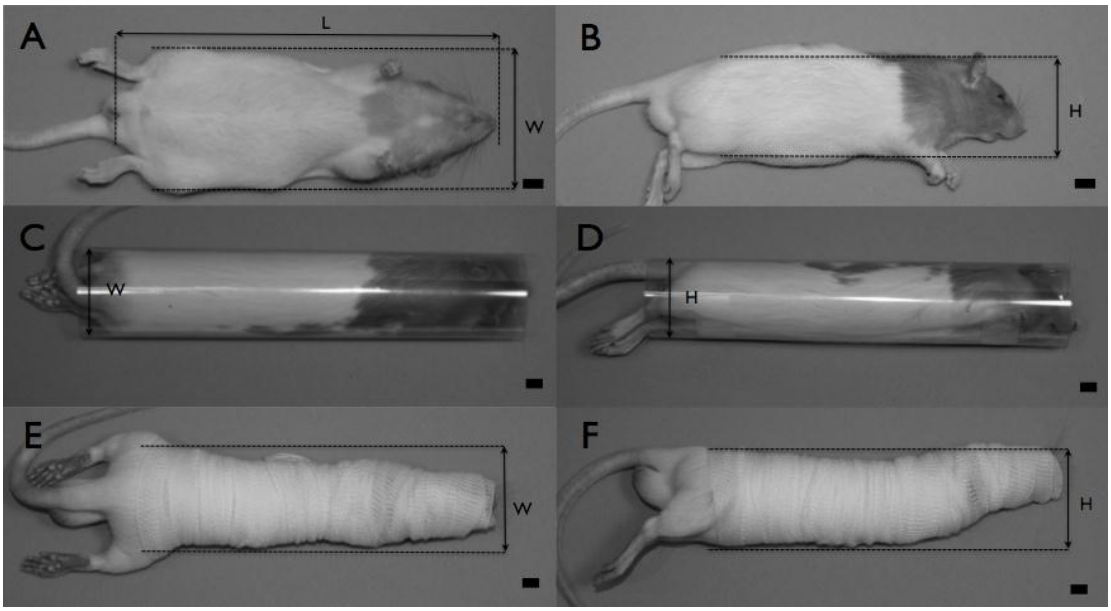

Figure 1. Photographs of a Norway rat with dimensions measured under different manipulations. *HW* is represented by A and B. A- Ventral view, B-Lateral view. *Ro* is represented by C and D. C-Dorsal view, D-Lateral view. Mylar used to allow prey to be viewed within cylinder. *Wr* is represented by E and F. E-Dorsal view, F-Lateral view. Scale bar=10mm.

Figure 2. Photograph a 1400g reticulated python (*Broghammerus reticulatus*) swallowing an 800g Norway rat at a late stage of oral transport (dorsal view).

displacement. To take volume readings rodents were dipped to the base of the tail after being completely immersed several times in a graduated cylinder to remove as much air as possible from the fur.

Analyses

Differences among means of cross-sectional area estimates derived from the four methods were tested with one-way ANOVA using PASW Statistics 18 for Windows. Raw data for both *Rattus* and *Mus* failed to meet the assumption of homogeneity of variance (Levene's Test) primarily because variances for *HW* and *Wr* were 2–6X times higher than those for *Ro* and *Vo* (Table 1). Therefore, data were log-transformed and homogeneity of variance was retested prior to the ANOVA. The log-transformed data for *Rattus* met the assumption of homogeneity of variance (Levene's test, $p>.05$) and differences among means were compared post-hoc using Fisher's Least Significant Difference (LSD) test. The log-transformed data for mice failed to meet the assumption of homogeneity of variance and differences among means were compared post-hoc using Dunnet's C test. To determine how the smallest cross-sectional area estimate (*Ro* method) scaled to mass and the various linear measures commonly used to measure rodents, we used reduced major axis regression (Sokal and Rohlf, 1995). All variables were log transformed prior to the analysis. Homogeneity of slope between variables was tested using methods reviewed by McArdle (1987).

Radiography

Taxon	Method	$\bar{x}$	S^2
Rattus	*HW*	1915	159 x 10^4
	Wr	1728	115 x 10^4
	Ro	1204	57.3 x 10^4
	Vo	955	31.5 x 10^4
Mus	*HW*	454	3.61 x 10^4
	Wr	454	2.10 x 10^4
	Ro	339	0.796 x 10^4
	Vo	289	0.608 x 10^4

Table 1. Summary of untransformed means and variances for cross-sectional area (mm^2) estimates derived by four methods.

An adult male rat was sacrificed using the methods previously described and X-rayed in lateral and ventral views—first in its resting state, and then after rolling it into a cylindrical shape (*Ro* method). To determine effects of ingestion on prey form, radiographs were also taken of a second adult rat (400g) following its ingestion by a 1400g reticulated python (*Broghammerus* [*Python*] *reticulatus*). To facilitate imaging in lateral and ventral planes, the python was anesthetized with 15mg/kg methanohexital 30 minutes prior to radiography.

RESULTS

Average cross-sectional area differed significantly across methods of measurement for both *Rattus* ($F_{(3,196)}$=10.18, p<.001) and *Mus* ($F_{(3,196)}$=14.29, p<.001). Post-hoc comparisons (Table 2) showed that average cross-sectional areas derived from *HW* and *Wr* methods were not significantly different (p=0.41 for *Rattus*, p=0.99 for *Mus*) despite the superficial impression that both the *Wr* method (Fig. 1E,F) and the effect of being swallowed (Fig. 2) similarly enlarged the caudal end of the prey relative to the head and body. In *Rattus*, average cross-sectional areas derived by both *HW* and *Wr* were higher than those by both *Vo* (p<.01) and *Ro* (p<.05). In *Mus*, average cross-sectional areas derived by *HW* and *Wr* were 1.5–2X higher than those by both *Ro* and *Vo* (p<.05 for all comparisons). Therefore values likely to be closest to ingestible size are those produced by the *Ro* and *Vo* methods.

Linear measures of mammals are inextricably tied to volume and mass, and change in any linear dimension should result in a change in cross-sectional area. Therefore, we determined the relationship between each standard linear measure (*HW*

Taxon	**Method**			
	HW	*Wr*	*Ro*	*Vo*
Rattus $\bar{x}$ (± SD)	3.19 (± 0.32)	3.14 (± 0.31)	2.99 (± 0.28)	2.90 (± 0.28)
Mus $\bar{x}$ (± SD)	2.61 (± 0.21)	2.63 (± 0.17)	2.51 (± 0.14)	2.44 (± 0.14)

Table 2. Means and standard deviations of log-transformed cross-sectional area (mm^2) estimates derived by four methods. Lines connect methods that are not significantly different using post-hoc Fisher's LSD tests for *Rattus* and Dunnet's C tests for *Mus*.

method) of a rodent and its cross-sectional area measured by the *Ro* method. Log cross-sectional area was highly correlated to log length in both *Rattus* and *Mus* and cross-sectional area scaled to length with positive allometry in each (Table 3, Fig. 3). Log cross-sectional area was also highly correlated to log height in *Rattus* (but not in *Mus*) and to log width in both taxa (Table 3, Fig. 3). Cross-sectional area scaled with positive allometry to both height and width in both taxa (Table 3, Fig. 3). Therefore, unless positive allometry is accounted for, all three standard linear measures alone overestimate ingestible prey size.

Mass is the most widely used measure of prey size, and its relationship to smallest attainable cross-sectional area is important because, unlike linear measures, the quantity is not affected by deformation. Log cross-sectional area was highly correlated to log mass for both taxa, and cross-sectional area scaled to mass with negative allometry (Table 3, Fig.4). Therefore, mass alone underestimates ingestible prey size.

Anatomy

X-ray images reveal that in the resting condition, the vertebral column is strongly curved with a ventral flexed region between the 6th cervical (C6) and 3rd thoracic (T3) vertebrae and a dorsal flexed region between T9 and the 1st lumbar vertebrae (L1) (Fig. 5A). A dorsal flexion also occurs between the head and C1. The *Ro* manipulation extends the head and vertebral column, decreasing the angle of the head by 20º and both vertebral curves by 45º. Maximal angular displacement between adjacent vertebrae was roughly 20º and occurred once at each vertebral curve (between T2 and T3 and T11 and T12 for curves 1 and 2 respectively). The straightening of the head and spine lengthens the body

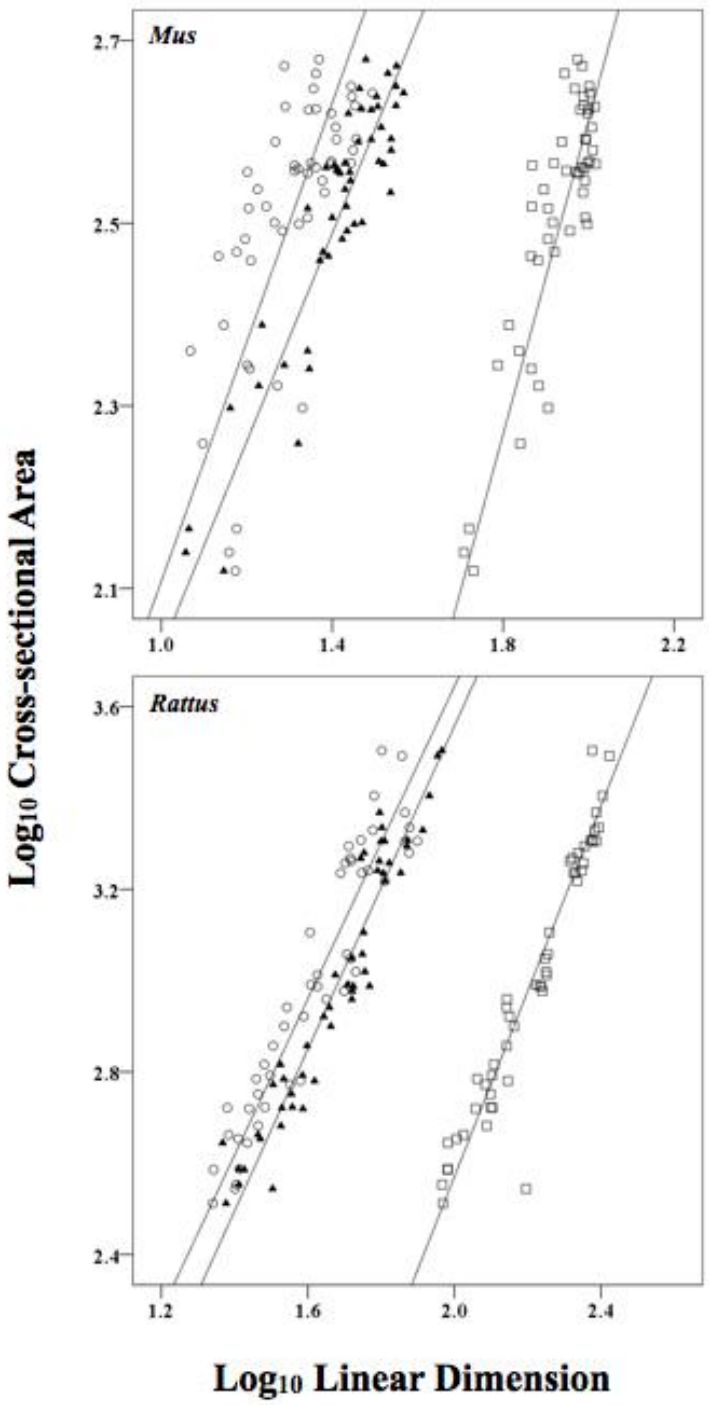

Figure 3. Plot of log-log relationship between single linear measures and smallest attainable cross-sectional area for *Rattus* (upper) and *Mus* (lower). □=length, ▲=width, ○=height.

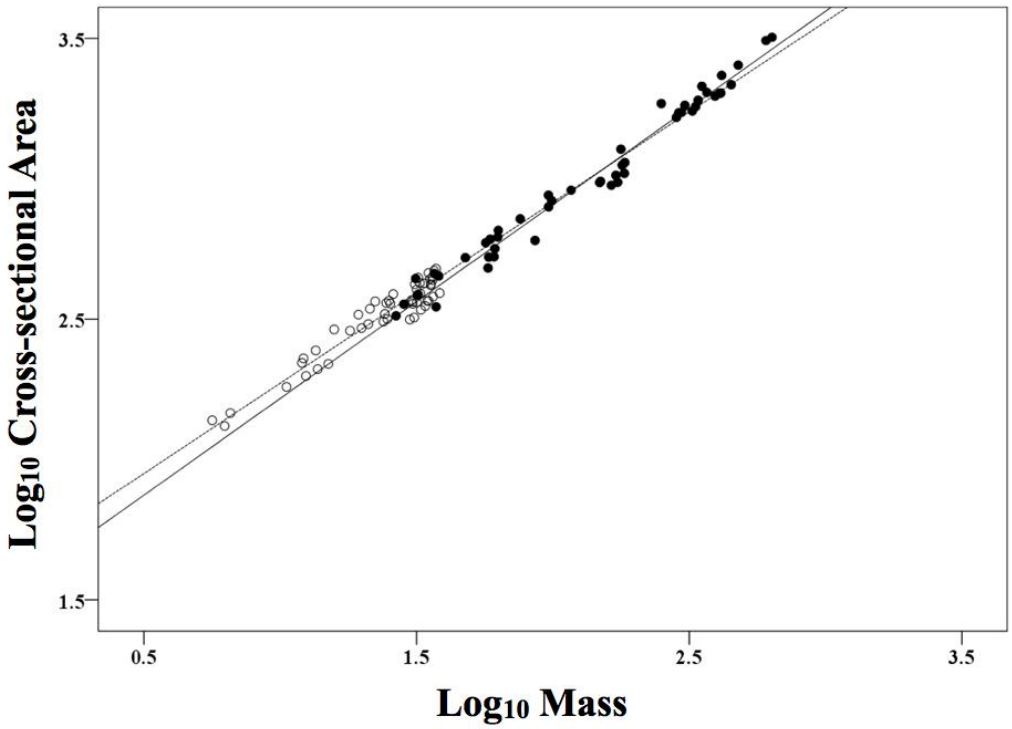

Figure 4. Plot of log-log relationship between smallest attainable cross-sectional area and mass of rodent prey. ●=*Rattus*, ○=*Mus.*

Taxon	Predictor	Slope (CI)	Y-int.	r^2	*P*
Rattus	Mass	0.69 (0.66–0.72)	1.53	0.98	<.05
	Length	2.03 (1.86–2.21)	-1.49	0.92	<.05
	Height	1.71 (1.55–1.89)	0.22	0.88	<.05
	Width	1.77 (1.63–1.93)	0.018	0.92	<.05
Mus	Mass	0.64 (0.59–0.70)	1.63	0.91	<.05
	Length	1.72 (1.48–2.00)	-0.83	0.73	<.05
	Height	1.31 (1.05–1.64)	0.80	0.40	<.05
	Width	1.14 (1.01–1.30)	0.89	0.82	<.05

Table 3. Reduced major axis regression analysis of log-transformed single predictors on log-transformed cross-sectional area for *Rattus* and *Mus*. *P* values indicate slopes differ significantly from 1.

(measured from the rostral tip of the nasal to the caudal edge of the 4th sacral vertebrae) by roughly 12% (Fig. 5C) and this is coincident with the caudal movement and redistribution of the thoracic and abdominal viscera. The sternum is elevated and the costal cartilages bend, decreasing the angle between the ribs and the vertebral column and compressing the thoracic cavity (Fig. 5A,C). The distal ends of the clavicles are protracted, bringing the shoulder joints cranially, and the forelimbs are pressed against the side of the body (Fig. 5B,D). The hindlimbs are adducted and extended caudally (Fig. 5A-D). These changes are similar to those seen in the rat inside the python (Fig. 5 E,F), a consequence of shaping done by the snake.

DISCUSSION

Previous attempts to measure mammals as prey have used size categories determined by pushing rodents through holes of specific sizes (Loop and Bailey, 1972; Shine, 1991). From our perspective this method generates two problems. The first is that this method does not actually measure the rodent, but simply generates size classes. The second is that pushing a rodent through a hole with "a modest amount of pressure" (Loop and Bailey, 1972) produces an estimate of cross-sectional area approximately 1.2–1.4X the value obtained by pulling the same rodent through holes with modest force. Mass is distributed caudally in both cases as the anterior trunk is compressed (Fig. 2, as for our *Wr* method), but our radiographs show that a rodent prey's mass is redistributed as it elongates during swallowing events (Fig. 5). Previous measures of smallest attainable prey diameter may have actually been closer to that of our *Wr* method, thereby overestimating ingestible size.

Shine (1991), although claiming to have used cross-sectional diameter as a measure of "effective size," actually used mass in all analyses because he found mass to be highly correlated with cross-sectional diameter. Mass is the most commonly used measure of size in the laboratory setting because it is highly correlated to linear dimensions, but it provides little information on the size of prey relative to the size of the predator's gape (Greene, 1983). Our data show that the smallest attainable cross-sectional area scales negatively to mass and the allometric relationship is slightly different for rats and mice. Therefore, in order for mass to be used as a measure of ingestible size, the scaling relationship has to be determined prior to the analysis.

Estimates of body size are obviously subject to methods of measurement and our data suggest that, for the same animal, different methods can generate significantly different average cross-sectional areas with variances that are also orders of magnitude different (Tables 1 and 2). However, our data also show that if good measures of length (Jewell and Fullagar, 1966) are combined with volume (as for our *Vo* method), cross-sectional area measures will be similar to those obtained by compressing a rodent into the smallest cylindrical mass possible (*Ro*) with similar repeatability (Table 1). Radiographs of rodents both rolled into cylinders and ingested by snakes indicate that *Ro* and, subsequently, *Vo* methods provide reasonable estimates of ingestible prey size, and we suggest that, when possible, either method be employed when measuring rodents as prey.

Measuring intact small mammals recovered from stomach contents of snakes provides the smallest attainable size of prey (Rodríguez-Robles et al., 1999a,b; Rodríguez-Robles, 2002; Glaudas et al., 2008) because ingested prey have been formed into cylinders during ingestion (see Fig. 6, Rodríguez-Robles, 2002). Our anatomical data

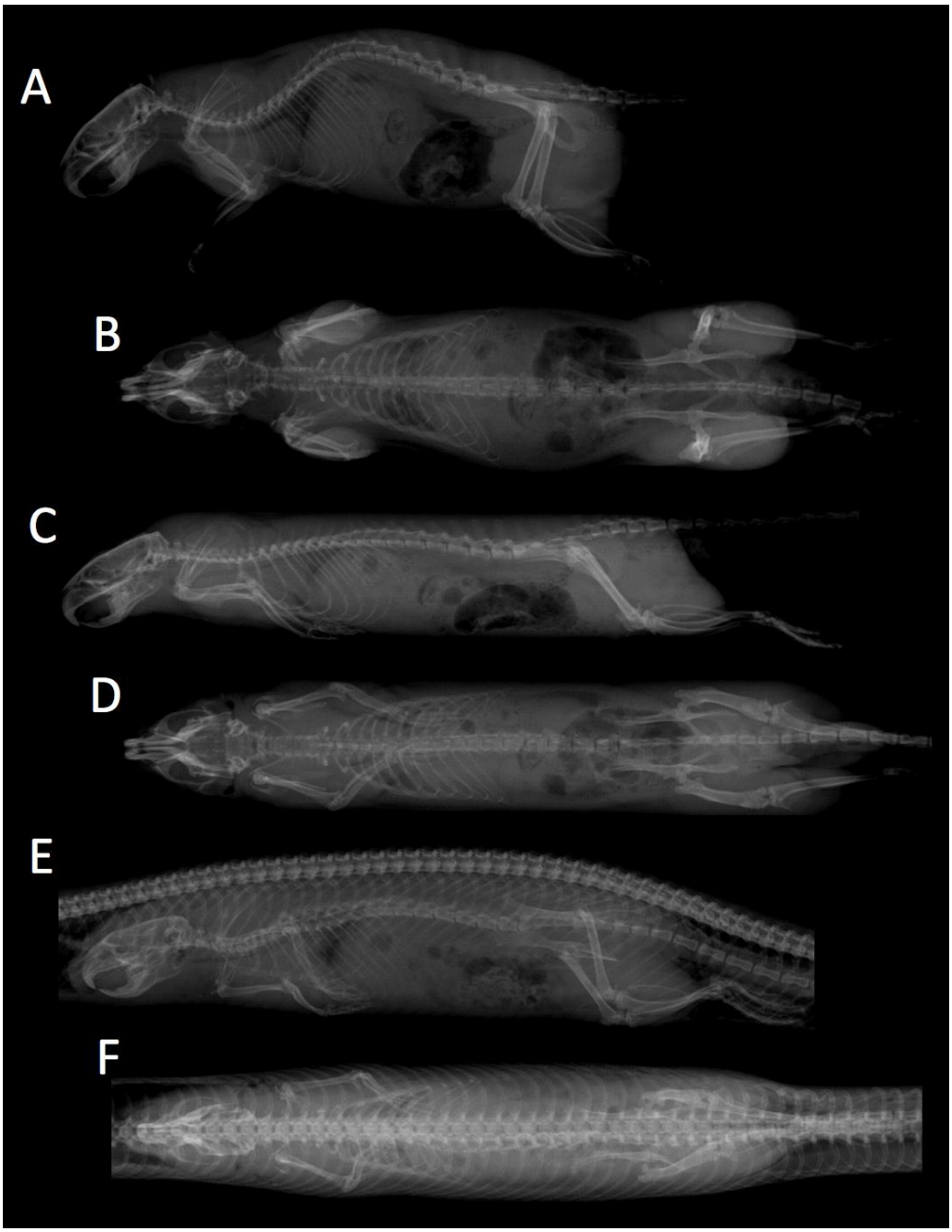

Figure 5. Lateral and ventral X-ray images of an adult Norway rat in both the *HW* (A,B) and *Ro* (C,D) conditions. Images E and F are lateral and ventral X-rays of an adult Norway rat showing the musculoskeletal changes that occur 30 minutes after engulfment by a reticulated python (*Broghammerus reticulatus*, shown).

suggest that if cross-sectional area was derived from height or width of prey from stomach contents, it should approximate the same values generated by our *Ro* method. Unfortunately, stomach contents are often not measureable and if species can be identified, measuring preserved conspecifics is commonly done (Rodríguez-Robles et al., 1999a,b; Rodríguez-Robles and Greene, 1999; Rodríguez-Robles, 2002; Fabien et al., 2004). Our results show that this practice is problematic because all linear measures of conspecifics potentially generate cross-sectional area estimates that are larger than ingestible size. While our *Vo* method would be convenient to use under these conditions, it is also a source of error because the length measurement required is dependent on the condition of the animal at time of preservation, how it was preserved, and the researcher's choice of landmarks (Jewell and Fullagar, 1966). However, if the scaling relationship between a mammal's linear dimension and its smallest attainable cross-sectional area is known (or determined as a part of the study), a single linear measure could accurately estimate ingestible size. We suggest using either *Ro* or *Vo* methods to derive smallest attainable cross-section areas of freshly killed conspecifics and then determining the allometric relationship between the desired linear predictor and smallest attainable cross-sectional area as a part of the study.

Prey width/diameter (Loop and Bailey, 1972; Pough and Groves, 1983; Shine, 1991) and height (Cundall and Deufel, 2006) can be used in conjunction with snake head dimensions to generate estimates of relative prey size. Snout-vent length is also used when prey type varies across vertebrate taxa (Vincent et al., 2005). Our data show that cross-sectional area estimates from height and width measurements of unmanipulated prey (*HW*) are higher and more variable than those of prey rolled into cylinders (*Ro*), and

smallest attainable cross-sectional area (using the *Ro* method) scales positively to resting linear dimensions (from the *HW* method). Therefore, to use any linear dimension as a measure of ingestible prey size, both the correlation coefficient and scaling relationship to smallest attainable cross-sectional area should be obtained for prey prior to the analysis. Fortunately, the laboratory setting is ideal for rolling prey into cylinders (*Ro*) or measuring length and volume (*Vo*), and our data provide the necessary information for two commonly used mammal species.

How snakes measure prey is currently unknown and there appear to be no published studies devoted to this problem (but see Weaver, 2010). That snakes can measure prey is assumed by most people who keep snakes. Discussions with numerous zoo keepers and curators and uncontrolled presentations of rodent prey of different sizes suggest that many snakes can detect relatively small differences in size, but whether snake responses are due solely to prey size differences remains unclear (Mori and Vincent, 2008). Owings and Cross (2008) showed that *Crotalus oreganus* selectively avoids large ground squirrels (*Spermophilus beecheyi*) even if they are capable of swallowing them. Direction of ingestion of mammals is highly correlated to prey size (Diefenbach and Emslie, 1971), and field experiments have shown that prey too large to ingest are usually avoided (Forsman and Lindell, 1993).

Multiple, interdependent modes of sensory input are used by snakes to orient their strikes and relocate prey after their strikes, but it has not been determined which modes are used to assess prey size (Kardong and Berkhoudt, 1999). Visual stimuli (particularly movement) are important in initiating foraging in numerous snake species (for review see Shine et al., 2004). Snakes appear capable of measuring relative distance to prey prior to

initiating their strikes (Cundall and Deufel, 1999), and limited field observations of *Crotalus horridus* suggest that relatively large prey species are eaten during the day as opposed to at night (Clark, 2006). Our data suggest that snakes using vision alone to assess prey would overestimate ingestible size. This might partly account for why snakes rarely attempt to capture mammals too large to swallow, though mistakes do occur (e.g., Rodríguez-Robles, 2002).

Two features of rodents that contribute to reducing cross-sectional area of the largest part of the body are the mobility of the clavicles and the potential for redistributing mass in the thoracic and abdominal cavities (Fig. 5). For snake predators, both features become relevant only when smallest attainable cross-sectional area of the rodent body approaches the maximal gape of the snake. At that point, rodents are invariably swallowed head-first and passing the rodent's shoulders through the angle of the jaw is possibly made easier by passing each shoulder sequentially. Rodent body mass is initially displaced caudally (Fig. 2), and continued engulfment by a snake gradually shifts rodent mass back towards the rodent's head. At the same time, snake gape and gut lumen cross-sectional area are gradually increased, providing ample time for snake gape and rodent cross-sectional area to equilibrate. Whereas the effects of shaping done by the snake on rodent prey are passive, the malleability of rodent bodies and the ability of mass to be shifted also provide the potential for increasing their apparent cross-sectional area as a defensive mechanism and for reducing it when burrowing. In studies of feeding performance of gape-limited predators that eat rodents, measurements of rodent size need to take malleability into account.

CHAPTER 3

Extensibility of Skin

INTRODUCTION

The integument forms the outermost layer of all metazoan bodies, and its form and function vary considerably (Brusca and Brusca, 2003; Kardong, 2012). In jawed vertebrates, it covers the jaw apparatus and must accommodate changes induced when the mouth is opened during feeding. In snakes, the mandibular symphysis in the lower jaw is highly modified or absent, one of a series of anatomical changes that allows them to swallow large prey whole (Gans, 1961; Kley, 2006; Young, 1998). The soft tissues linking the mandibles determine how far the mandiblular rami can separate, and this distance determines overall gape size (Arnold, 1983; Cundall and Greene, 2000). To allow separation of the mandiblular rami, the skin must be either extensible or loosely connected to each mandible.

The basic morphology of squamate skin was described previously by Ficalbli (1888), Lange (1931), Pockrandt (1937) and Maderson (1964). To summarize, the epidermis of snakes consists of scale and interscale (*hinge* of Maderson (1964) and Mittal and Singh (1987b), *inner scale + hinge* of Alibardi and Thompson (1999), or *intersquamous* of Savitzky et al. (2004) and Rivera et al. (2005)) regions that are continuous. Both regions consist of a stratum germinativum composed of cuboidal (interscale) or columnar (scale) cells on which rest one to several layers of differentiated (scale) and/or presumptively undifferentiated (Mittal, 1987b) living cells (*cellules à mamelon* of Ficalbi, 1888). As in other vertebrates, the cells of the stratum germinativum are anchored to the basement membrane at their basal surfaces via hemidesmosomes

(Roth and Jones, 1967) and to neighboring cells at their lateral and apical surfaces via desmosomes (Roth and Jones, 1967). The scale regions consist of an α layer (α-keratin), a mesos layer, a β layer (β-keratin), and finally a thin superficial Oberhäutchen. The scale epidermis has received the most attention in the literature, mainly within the contexts of development (Alibardi, 2002; Alibardi and Thompson, 2003; Maderson , 1965b; Swadżba and Rupik, 2010) the shedding cycle (Maderson,1965b; Mittal and Singh, 1987; Roth and Jones, 1967; Roth and Jones 1970) and micro-ornamental specializations in scale Oberhäutchen (Chiasson and Lowe, 1989; Gower, 2003; Irish et al., 1988; Joseph et al., 2007; Price, 1982). The scales also house the major epidermal sense organs of the skin (Jackson and Sharawy, 1980).

The interscale region was described by Ficalbi (1881), Maderson (1964) and Pockrandt (1937) but has received relatively little attention in the literature since. It was the primary subject of a single study on the shedding cycle (Mittal and Singh, 1987b), but in most studies of the shedding cycle (Maderson, 1965a; Mittal and Banjerjee, 1980; Roth and Jones, 1967; Roth and Jones 1970) or skin development (Alibardi, 2002; Alibardi and Thompson, 2003; Swadżba and Rupik, 2009; Swadżba and Rupik, 2010), it is only briefly mentioned. To summarize, the interscale epidermis of squamates is thrown into folds that are thought to serve a variety of functions (Jackson and Reno, 1980; Lillywhite and Maderson, 1982; Maderson, 1964; Roth and Jones, 1967; Sherbrooke and Scardino, 2007). The interscale epidermis shares most layers with the scale region but lacks the β-layer (and thus most of the hard β-keratins that give the scale region its stiffness), and the mesos and α-layers are thin and difficult to distinguish. The Oberhäutchen is thin and the surface is characteristically bumpy. The keratins of the

interscale region are predominantly α-keratins, and it is thought that the region should be much more compliant than the scale regions. Thus, if the epidermis of snakes is an extensible stratified squamous epithelium, the structure and function of interscale regions should be critical to its behavior.

Reviews and discussions of the structure and function of the vertebrate dermis have illustrated the importance of its organization and composition to the mechanical behavior of the whole integument (Montagna, 1962; Moss, 1972; Montagna et al., 1970). Despite this, and the apparent accepted phenomenon of skin extensibility in snakes, descriptions and discussion of the dermis in snakes are scarce. Pockrandt (1937), Roth and Jones (1967) and Jackson and Reno (1975) recognized both dermal and epidermal components to snake scales, pointing out that the dermis is thickest near the center of the scale and thinnest near the lateral and caudal free margins. Maderson (1965b) and Alibardi (2002) described the development of the dermis in the outer and inner [marginal] scale surfaces and hinge regions of lizards and snakes, but unfortunately provided no details on the interscale region. From these studies, it is clear that the dermis of the scale region consists of at least two layers, a thick, superficial *stratum laxum* of loosely organized collagen and uniformly distributed mesenchymal fibroblasts and a deep *stratum compactum* composed of dense, parallel-fibered collagen and flattened, randomly distributed fibroblasts. Licht and Bennett (1972), in their study of a scaleless *Pituophis melanoleucus catenifer*, showed that the superficial dermis was entirely absent in scaleless specimens and that this component was the "major morphological element" of the scale. Alibardi (2002) also recognized a third layer of "loose" subdermal reticular fibers that are apparently orthogonal to the axis of the scale (see Fig. 9 from Alibardi,

2002). The latter suggests that the dermis of late-stage snake embryos possesses a structurally and functionally divided dermis, though the structure is not well described and the functions are speculative.

If we assume that the dermis of snakes is similar to other vertebrates in its structure and composition (which would be the exact opposite of the epidermis), it should be composed, in order from most to least abundant, of ground substance, collagen, fibroblasts and elastin. Also, although aforementioned studies showed that the dermis is structurally divided between scale and interscale regions, only Pockrandt (1937) distinguished collagen and elastin in the two regions and therefore ascribed hypothetical mechanical functions to each region. To date, two published studies on the tensile properties of snake skin (Jayne, 1988; Rivera et al., 2005) and one unpublished account (Savitzky et al., 2004) have placed the dermis as a key structural element to snake skin extensibility, and have attempted to relate these components to the skin's behavior. Unfortunately, to date no study has shown which parts of the snake integument define the limits to its extensibility and none has provided a mechanism for passive recovery from highly extended states. Given the established structure and function of elastin (Debelle and Tamburro, 1999; Oxlund et al., 1988; Partridge, 1970), it is likely (as was suggested by Savitzky et al., 2004 and Rivera et al., 2005) that elastin in the dermis is responsible for the refolding of interscale skin and subsequently for returning the skin to its resting condition after stretch. Therefore, as was suggested previously by Montanga (1962) and Partridge (1970), the elastin in the deep dermis should be responsible for skin's elastic behavior.

The skin and intermandibular soft tissues determine the lower jaw's extensibility. Because the upper jaws are less extensible, lower jaw extensibility is a major determinant of gape in snakes (Arnold, 1983; Cundall and Greene, 2000). Within the context of macrostomy, we examined how skin behaves during swallowing and then related function to structure. We first asked how the scale and interscale regions of lower jaw skin responded to stretch during swallowing events. Based on previous descriptions of skin morphology and previous studies of skin's mechanical behavior, we predicted that during swallowing events, lower jaw scale width would not increase between resting and maximum gape, but that distances between adjacent scales, and therefore interscale skin, should increase. Secondly, we asked how our behavioral results related to gross and microanatomy by both qualitatively and quantitatively describing the changes that occur between resting, moderately stretched and highly stretched lower jaws. Specifically, we predicted that although gross anatomical effects would be seen at levels of moderate stretch, only the highly stretched condition might be characterized by major histological and cytological changes. Finally, we asked which epidermal and/or dermal features define the structural limits to interscale skin extensibility and sought to provide a model for the skin's passive recovery following stretch.

METHODS

Animals

Northern watersnakes (*Nerodia sipedon sipedon*) were collected locally, housed in the laboratory on a 12:12-hour light:dark cycle at 25-28°C, and given access to water *ad libitum*. Neonates born in the lab were reared under the same conditions. Adult snakes

were fed shiner minnows (*Notemigonus crysoleucas*) and trout (*Oncorhynchus mykiss*, *Salmo trutta*, and *Salvelinus fontinalis*) every 7-10 days and neonates were fed fathead minnows (*Pimephales promelas*) every 4-7 days during the study.

Feeding behavior

Prior to feeding trials, snakes and prey were weighed and mass ratios (calculated as prey mass/snake mass) were obtained. Maximum height and width of the fish were measured, and these values were used to calculate prey cross-sectional area (calculated as the area of an ellipse using the equation: [π x height x width]/4). Prey cross-sectional areas (CSA_{Prey}) were combined with estimated cross-sectional areas of gape (CSA_{Snake}) derived from snake jaw lengths ([π x JL^2]/4, JL measured as the distance from the anterior border of the mental scale to the caudal edge of the bulge formed by the retroarticular process of the mandible) in order to calculate ingestion ratios (calculated as CSA_{Prey}/CSA_{Snake}).

Neonates were fed in an arena that consisted of a glass plate floor with a mirror angled at 45° below, allowing for simultaneous lateral and ventral views of snakes during feeding (Fig. 6). Larger adults were fed in a larger feeding arena used previously by Cundall and Deufel (2006), allowing for similar views of larger specimens. All behavioral records were collected using either a Panasonic AG-456 VHS recorder or Cannon ZR900 miniDV camcorder. VHS records were analyzed by playing back tapes on a TV monitor and measuring distances directly on the monitor with a ruler. All miniDV records were captured and edited using FinalCut Pro software (Apple Computer,

Inc.). Still frames were analyzed using Image J software (National Institutes of Health, Bethesda, MD).

Video records of feeding (Table 4) were analyzed for dynamic changes in skin during feeding trials. In lieu of marking animals prior to feeding trials, digital markers were placed at points along the median and lateral margins of genials (G_R,G_L) and anterior chin shields (A_R,A_L) from still video frames (Fig. 7A,B). For the genials we placed a point directly anterior to a distinct 135° bend in the medial margin, and then placed a second point on the lateral margin at the end of a line that originated at our first point and was orthogonal to the lateral margin of the scale. For digitally marking the anterior chin shield, we first placed a point on its medial margin directly behind the overlapping posterior free margin of the genial. We then placed a second point on the lateral margin at the end of a line drawn from the first point orthogonal to the lateral margin. This region was chosen because, from a superficial view, it was the only region where data on two-scale relationships can be accurately obtained and where interscale distances could be measured easily *in vivo* without marking scales prior to the feeding trial. All other scales of the lower jaw overlap, and thus the lateral margins of adjacent scales are impossible to see in the resting condition.

The distance between markers was measured at rest either prior to or immediately following a swallowing sequence and at the largest gape recorded. The latter occurred when both gape angle (measured as the angle formed between the braincase and the lower jaw axes) and intermandibular distance (measured as the distance between the tips of the mandibles) were at their highest values. Univariate linear regression was used to

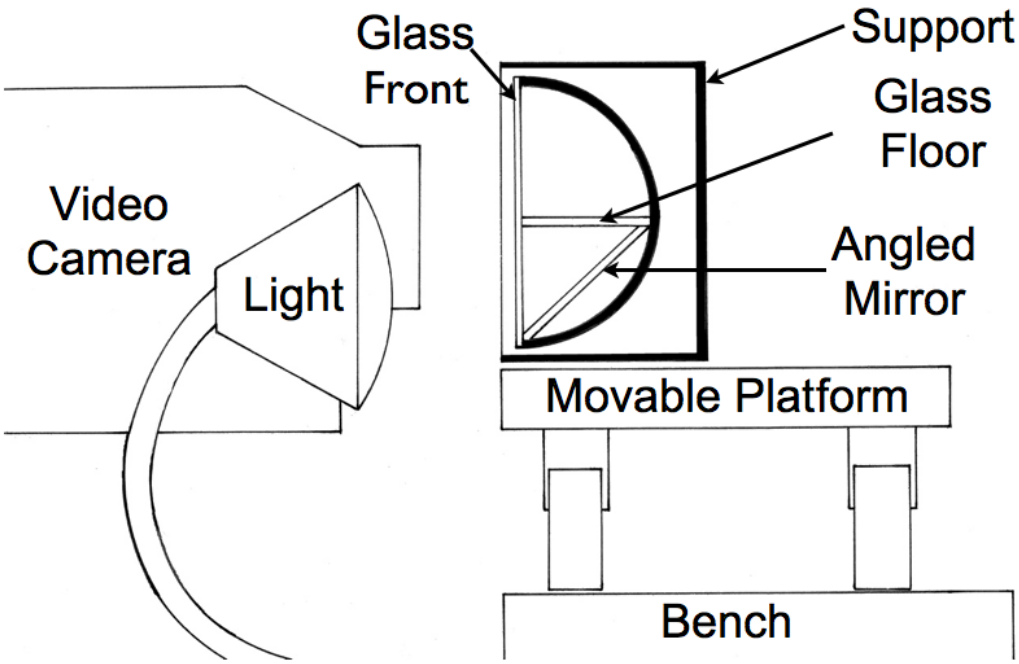

Figure 6. Diagrammatic view from the right end of the feeding arena used for neonate water snakes. The arena was made of a 14” length of 1.5” PVC pipe cut in half and supported by wooden blocks. The mirror and glass pieces were fit into grooves cut in the wooden support panels. The entire arena sat on a rolling dolly positioned immediately in front of the video camera and light source.

Individual	# Trials	Mass Ratio	CSA_{Prey}/ $Gape_{Estimated}$
Adult 1	1	30%	62%
Adult 2	5	35-84%*	75–107%*
Adult 3	1	46%	45%
Adult 4	3	32-90%*	52–109%*
Neonate 1	4	30-44%	41–60%
Neonate 2	5	30-59%	46–63%
Neonate 3	4	32-40%	40–50%
Neonate 4	1	37%	45%
Neonate 5	1	39%	59%
Neonate 6	6	30-45%	37–92%
Neonate 7	5	34-53%	36–63%
Neonate 8	6	32-58%	27–78%
Neonate 9	5	31-57%	39–70%
Neonate 10	1	31%	38%
Neonate 11	1	45%	41%
n=15	**n=49**	**30-90%***	**27-109%***

Table 4. Summary of Behavioral Records for *Nerodia sipdeon*. Individuals in bold are those later used for anatomical and/or histological analyses. Values for ratios are ranges.

* denotes an event in which an attempt was made by the snake to ingest prey, but regurgitated after maximum gape had been achieved.

scale change in intermandibular distance to ingestion ratios (Fig. 7C). All values measured from video records were scaled to known distances from the feeding arena. To correct for differences in size between individuals, values were scaled to lower jaw length.

Changes in distance between markers were compared between scale and interscale regions, and data were analyzed using a two-way ANOVA, testing for interactions between treatment group (resting versus stretched) and skin region (scales versus interscale).

Mechanical Testing

Uniaxial tensile tests were carried out on two adult watersnakes in order to determine the loads attained when the mandibles were extended under conditions similar to those seen during feeding trials. To do this, snakes were anesthetized with 30mg/kg of pentobarbital and their mandibles were secured in clamps designed by DC that gripped the mandibles while allowing the skin and soft tissues lateral to the mandibles to roll through the clamp as strain increased. The clamps were fixed in an INSTRON 5567 tensile testing machine fitted with a 500N load cell.

Extension limits were initially set at 7X resting snake intermandibular distance, and extension was applied at a ramp rate of 0.0167 mm/s. To simulate swallowing-like behavior for our mechanical tests, we programmed periods of rest that started with 30 sec and gradually increased to 300 sec as extension increased. Therefore, the total time for a mechanical test varied from 45min to 1 hour depending on the individual tested. The interior of the mouth was irrigated with water during testing to prevent the mucosa from

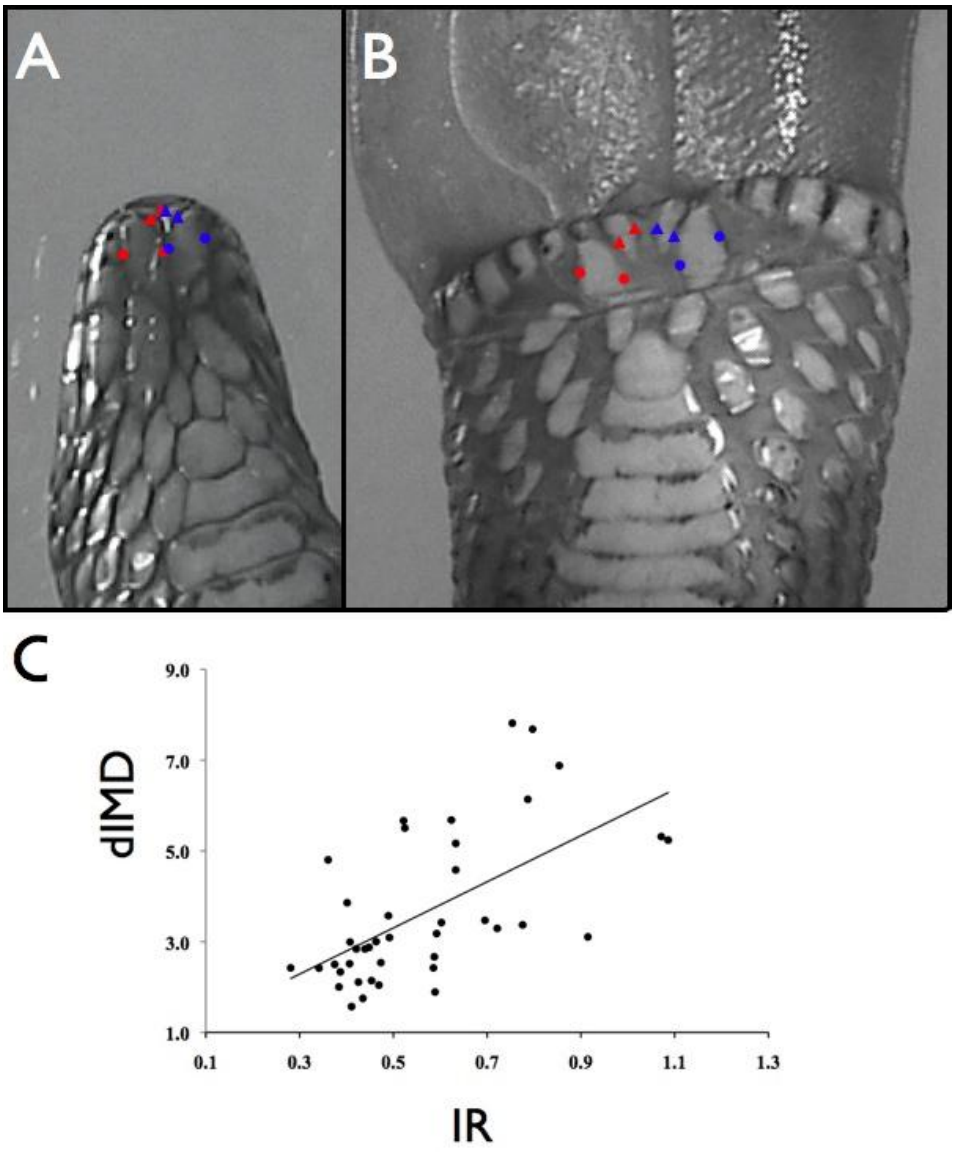

Figure 7. A–B) Still frames captured from video of a Northern watersnake swallowing a trout 40% its body mass. A. Ventral view of head at rest. Markers indicate the borders of the right (red) and left (blue) genials (▲) and anterior chin shields (●). B. Ventral view of head at maximum gape, with markers as in A. The width of scales increases slightly and significantly upon stretch, but the increase is significantly smaller than the increase in distance between scales. C) Plot of ingestion ratio (x) on change in intermandibular distance (y) during feeding trials.

drying. Snakes recovered following the tests and regained normal feeding activities. A second trial was conducted on one individual after four months, and the extension limit was increased to 10X resting intermandibular distance.

Mechanical Manipulations for Anatomical and Histological Preparations

Specimens were anesthetized with isoflurane, received one of three treatments, and were sacrificed by overdose with anesthesia or by decapitation following anesthesia. One group received no treatment (although the oral cavity was opened slightly to allow the mouth and gut to be flooded with fixative) and was fixed in the resting condition with 10% phosphate-buffered formalin. Intermandibular distance was measured using either dial calipers or, for smaller snakes, an ocular micrometer or miniscale (Microtool,TM).

For the stretch treatment groups, the right mandible was pinned to a dissecting tray using hooks fashioned from 00 or 0 insect pins, and the left mandible was gripped with forceps and extended laterally to approximately 2X its resting distance. The left mandible was then pinned and allowed to rest for a period of five minutes. It was then unpinned and subsequently extended to 3X resting distance. For Moderately Stretched (MS) specimens, the lower jaws were fixed between 3 and 5X resting distance. For Highly Stretched (HS) specimens the process of rest and extension was repeated over periods of 20 min-1 hr until the mandibles were between 5 and 7X resting distance. This was done to simulate normal physiological conditions, ensuring that the mandibles were extended to ranges seen in behavioral records of snakes feeding on the largest prey taken and to allow time for the soft tissues to adapt to the strain. Each animal was then fixed in the stretched condition with 10% phosphate-buffered formalin.

Anatomy

Lower jaws were removed from fixed specimens and stored in 70% ethanol. In order to obtain detailed anatomical information on lower jaws prior to further processing, specimens were drawn, photographed and/or measured using either an ocular micrometer or a miniscale. The following measurements of scales (Fig. 8) were collected in order to compare resting with stretched specimens: DMG, distance between mental and genial scales; DGG, distance between genial scales; DGA, distance between genials and anterior chin shields; DAA, distance between anterior chin shields; $DAL_{3,4,5}$, distance between anterior chin shields and infralabials 3, 4 and 5; DPP, distance between posterior chin shields, $DPL_{5,6,7}$, distance between posterior chin shields and infralabials 5,6 and 7. Scales were measured from the approximate center of each scale, defined as a point midway between anterior and posterior borders and lateral and medial margins.

Resting, moderately stretched and highly stretched specimens were used for microdissection (Table 5). The skin was removed carefully from the level of the jaw joint, working rostrally towards the genial scale. Complete removal of the skin could not be accomplished without removing important intermandibular connective tissues, and the skin was reflected at the most anterior point possible (without destroying these tissues) at the mental scale. Removal of the skin required severing of several distal branches of the the trigeminal nerve innervating the scales. Therefore, intact networks of major nerves innervating the scales were identified using a small sample of cleared and stained specimens (Table 5; Nishikawa, 1987). Once identified, we were able to compare intact networks with severed branches attached to the dorsal surface of the skin and better identify neurovascular bundles and their attachments to the skin. These were then

Sample Type	Treatment Group		
	Resting	Moderately Stretched	Highly Stretched
Anatomical	Neonate 12 **Neonate 1**[CS] Neonate 13 Neonate 14[SEM] **Neonate 7** Neonate 15[CS] Adult 5[SEM]	Adult 4 **Neonate 2** **Neonate 5** **Neonate 10** Adult 6	Neonate 16[SEM] Neonate 17* Neonate 18[CS] **Neonate 6** Adult 7 Adult 8[SEM]
n=18	n=7	n=5	n=6
Histological	Neonate 19 Neonate 20 Neonate 21 Neonate 22 Neonate 23 Neonate 24	Neonate 25 Neonate 26 Neonate 27	Neonate 28 Neonate 29
n=11	n=6	n=3	n=2

Table 5. Summary of anatomical and histological samples examined.
[CS] specimens that were cleared and stained
[SEM] specimens prepared for scanning electron microscopy
* specimen that was stretched to the point of failure

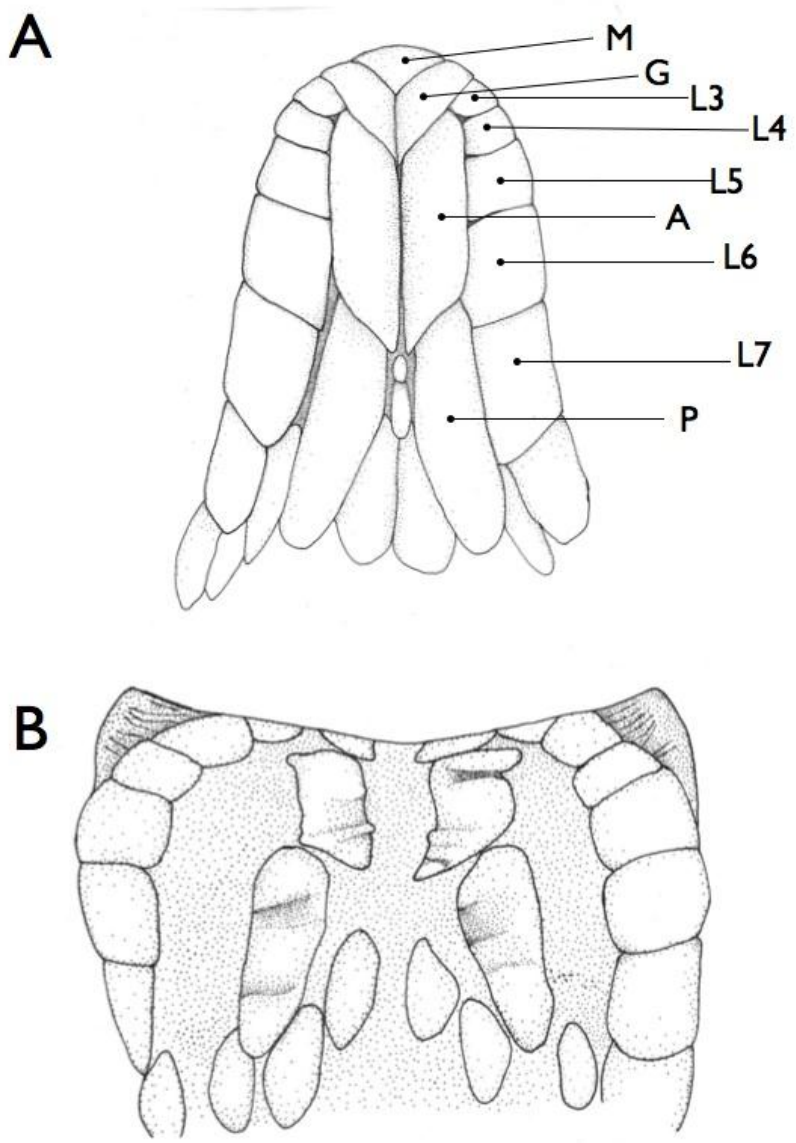

Figure 8. Superficial view of resting (A) and stretched (B) lower jaw skin. Scale nomenclature as shown in (A): A–Anterior Chin Shield, G–Genial (infralabial 2), L3—L7–Infralabials 3–7, M-Mental (infralabial 1), P–Posterior Chin Shield. In B, the mental and half of the genial scales are not visible because the skin is curved dorsally and posteriorly.

mapped and compared for both resting and stretched specimens.

Histology

Resting, moderately stretched and highly stretched specimens (neonates and juveniles) were prepared for light microscopy (Table 5). Samples were dehydrated through a series of graded ethanols, cleared in xylene and embedded in paraffin. Blocks were sectioned at 5-10mm, and sections were mounted into three series. Each series was stained with H&E, iron gallein elastin stain (Churukian and Schenk, 1976), or Masson Trichrome (Humason, 1979) for connective tissues. Resting and stretched specimens were then examined using a Nikon Eclipse 50i compound light microscope (Nikon Corporation, Japan) fitted with a Nikon Digital Sight DS-5M CCD camera (Nikon Corporation, Japan). All measurements were made using a Nikon Digital Sight DS-L2 control unit (Nikon Corporation, Japan).

In order to determine the histological effects of stretching, scale and interscale regions were compared at two locations from anterior snake lower jaws. The first region consisted of the area between and including anterior chin shields and the second comprised the region between and including the anterior chin shield and adjacent labial scales. Effects of stretching on the superficial epidermis were difficult to determine because the keratinized layers tended to be at least partially removed either during dehydration or during sectioning. In addition, because time since shedding had not been established prior to sample preparation it was difficult to assess how and whether the shedding complex influenced stretch treatment.

Effects of stretching on the epidermis were quantified using the following set of variables: 1) Fold amplitude, FA, was measured as the amplitude of the major folds of interscale skin. FA was only measured for interscale skin because folds do not appear in the scale regions. A minimum of three folds were measured from both sample areas in each section, and a total of five sections containing each region of interest were analyzed and averaged. Therefore, a total of 60 samples from each area were averaged for resting and stretched treatment groups. 2) Internuclear spacing of stratum germinativum cells, EINS (Fig. 9), was measured as the linear distance between a pair of adjacent nuclei of the stratum germinativum. A total of 10 pairs of nuclei was sampled for scale and interscale regions in each section, and 5 sections were averaged from 4 specimens each, to yield a total of 200 points for scale and interscale regions of each area sampled in unstretched and stretched treatment groups.

Since the vertebrate dermis is a composite tissue containing primarily collagen, ground substance, elastin and fibroblasts (Gibson and Kenedi, 1970) and since the dermis is distinctly different in composition along its depth, we first determined its relative elastin composition using differential point counting of serial sections. To accomplish this, serial sections of dermis were selected and a digital 100-square grid was overlain over the image in the microscope's control unit. Each cell of the grid was then scored as being primarily composed of elastin if elastin made up more than 50% of the total area of relative composition along the depth of the dermis, from superficial dermis to the deep dermis, in each region. We then compared scale and interscale regions of dermis for the two areas sampled.

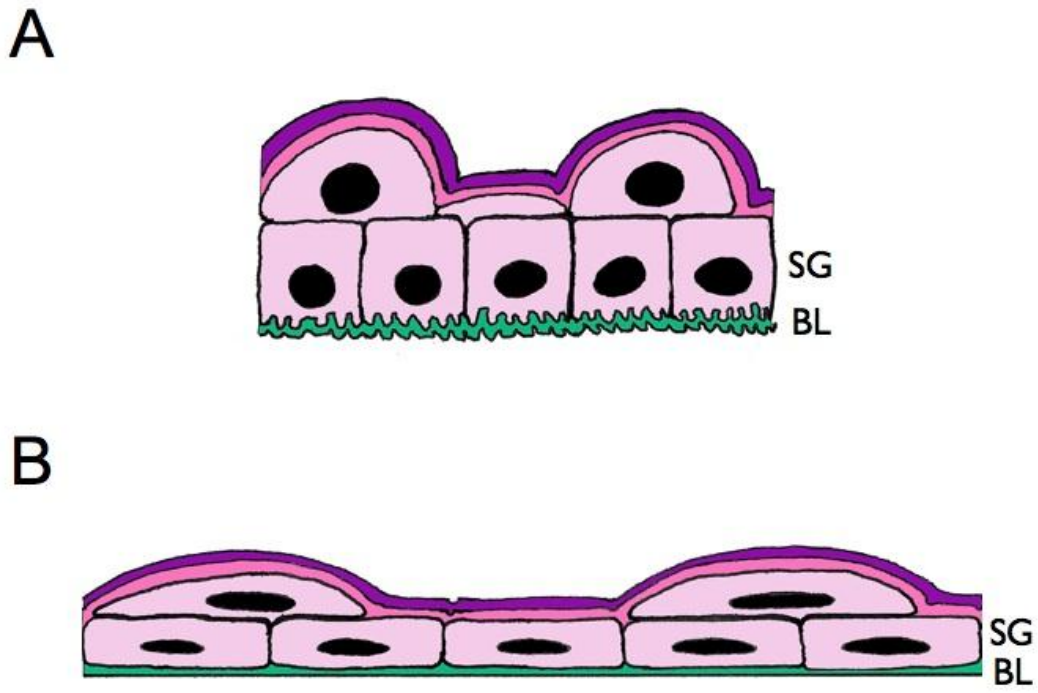

Figure 9. Internuclear spacing in the epidermis (EINS). A. Resting condition. B. Stretched condition. In the resting condition, the basal lamina (BL, green) and adjacent cell membranes are convoluted. Cells of the stratum germinativum (SG) are anchored to the BL via hemidesmosomes, and are anchored to adjacent cells via desmosomes. Therefore, when the epithelium is stretched, the BL unfolds and the SG cells lengthen in the direction in which load is applied. This causes a decrease in the cross-sectional area of cells an increase in the distance between nuclei of adjacent cells, which serves as a relative indication of the strain of the epithelium.

As in most vertebrates, collagen fiber distribution and orientation were distinctly different between superficial and deep dermis. Therefore, we characterized fiber orientation/arrangement as being transverse/parallel, transverse/woven, or orthogonal, and noted orientation changes between resting and stretched specimens. Because the quantitative effects of stretch on collagen are difficult to determine with the light microscope, we quantified the effect of stretch on the dermis using dermal fibroblast internuclear spacing, DINS. Our use of measuring DINS was underlain by the assumption that as the extracellular matrix changes during mechanical events, fibroblasts will stretch in the plane of extension. While cytoplasmic processes are not easily distinguished, the nuclei are relatively distinct and should give an approximation of how far fibroblasts stretch during extension events (Fig. 10). DINS was measured for 10 pairs of fibroblast nuclei from the superficial and deep dermis of the scale region and the dermis of the interscale region for five sections from each region sampled.

Scanning electron microscopy

A small sample of resting and stretched specimens was used to compare regional differences in response to stretch using scanning electron microscopy (Table 5). Skin was removed from the lower jaw and the medial margin of the right anterior chin shield was removed to expose the interscale epidermis. The left anterior chin shield's right margin remained intact. Samples were dehydrated through a series of graded ethanols, air dried, and mounted to stubs with conductive tape. All samples were then viewed with a Hitachi TM-1000 scanning electron microscope. From images collected using the computer's viewer program, we subsequently measured major and minor axes of 50 resting and 50

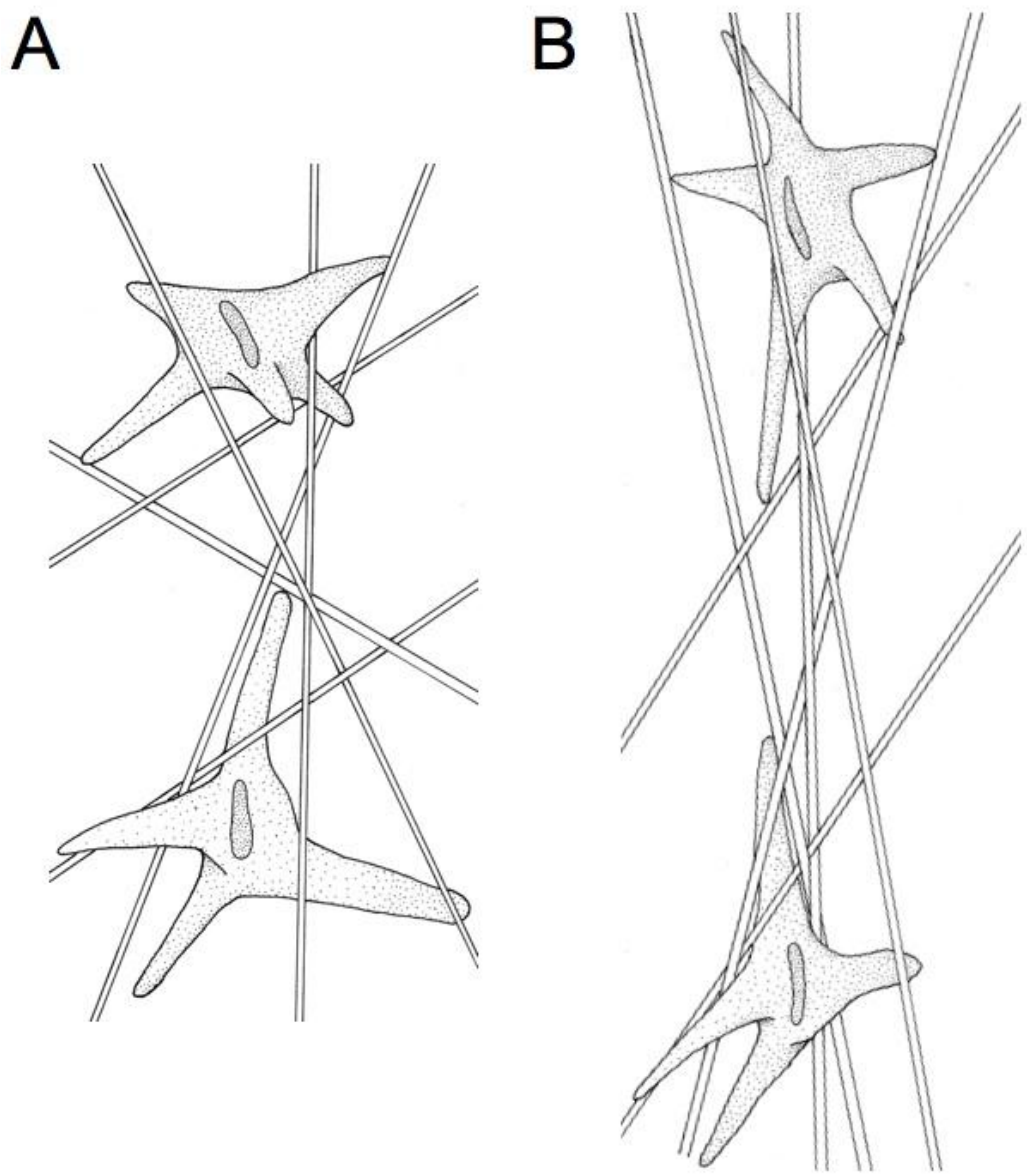

Figure 10. Dermal fibroblast internuclear spacing (DINS). A. Resting condition. B. Stretched condition. As the collagen fibrils in the extracellular matrix are reoriented, the fibroblasts migrate and/or are stretched in the direction in which the load is applied. The distance between adjacent fibroblast nuclei therefore gives a relative measure of strain of the extracellular matrix during a mechanical event.

stretched *cellules à mamelon* (Ficalbi, 1888), a large, superficial, presumably undifferentiated cell (Mittal and Singh, 1987) of the interscale region, using Image J software.

All methods were approved under Lehigh University IACUC Protocol 66.

Statistical Analyses

Differences in our set of scale—scale distances among treatment groups were tested using a one-way multivariate analysis of variance (MANOVA). Univariate, pairwise Fisher's LSD comparisons were then used to determine how individual pairs of scales differed under each treatment and which pairs were consistently different between treatments. Differences in each of our histological variables among treatment groups were tested using multiple one-way ANOVAs, and in cases where histological variables were shared between scale and interscale regions, we instead used two-way factorial ANOVAs to test for interactions between treatment and region. In all cases, pairwise Fisher's LSD comparisons were used to test for significant differences among groups. All statistical analyses were conducted using PASW Statistics 18 software package (IBM Corp.).

RESULTS

Feeding Behavior and Mechanical Testing

Relative prey sizes used in this study ranged from 30-90% for mass ratios and 27-109% for ingestion ratios (Table 4). Gape angle ranged from 41°-62°, intermandibular

distance ranged from 2.5-7.7X resting distance, and time to reach maximum gape occurred between 8 and 20 minutes after swallowing began. These results provided the data used to establish both the parameters of mechanical testing as well as experimental manipulations used for determining skin function.

The maximum loads imposed on the intermandibular soft tissues *in vivo* was 1.9N, occurring at 10X resting intermandibular distance (Fig. 11A,B). Introducing rest periods into the test extended the total time that the tissues were extended but also allowed for time for the tissues to adapt between increases. Therefore, within each period of increase the load vs. extension increased sharply, whereas the increase overall was slow and more linear (Fig. 11B). In none of the mechanical tests did the lower jaws reach failure, and both animals tested recovered fully. In combination with our behavioral measures, these results show that the absolute limit to lower jaw extensibility was 1) greater than in any of our feeding trials (10X resting IMD as compared to 7.7X resting IMD) and 2) a time-dependent process.

Behavior of Skin In Vivo

In order to determine how skin regions (scale, interscale) responded differently to passive loads applied under normal physiological conditions, we compared the difference in distances within (scale width) and between (interscale distance) scales from two pairs of scales (genials [G], anterior chin shields [AC]) at resting and maximum achieved gape during swallowing events using two-way ANOVA. Data are provided in Table 6. Average scale width increased by 22% for genials and 18% for anterior chin shields ($p<0.05$), and interscale distance increased by 307% between genials and 437% between

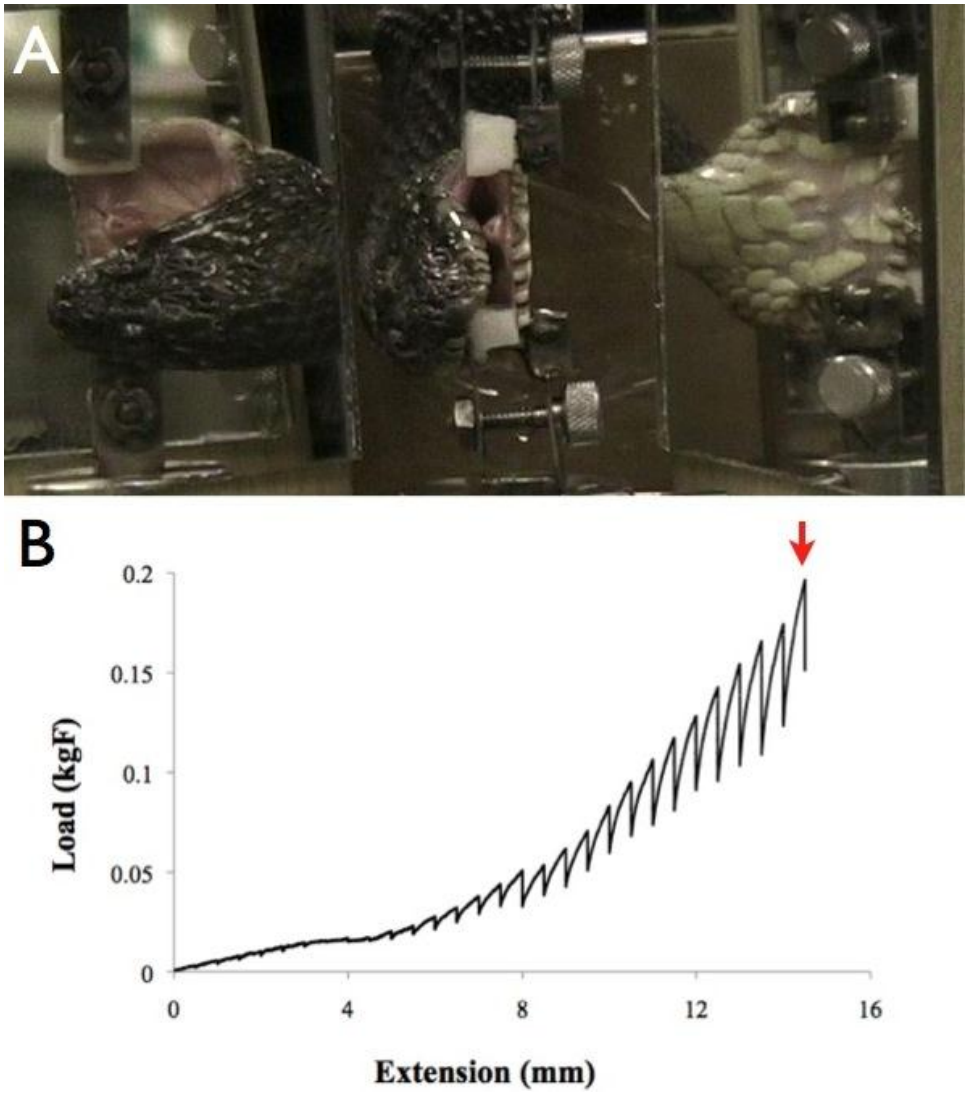

Figure 11. Mechanical testing of intermandibular soft tissues. A) Dorsal (left), rostral (middle) and ventral (right) views of an adult watersnake in mechanical testing apparatus at maximum extension. B) Plot of load vs. extension data for the individual shown in A. Red arrow indicates point at which 10X intermandibular distance (measured from resting intermandibular distance) was achieved.

anterior chin shields ($p<0.05$). Interscale regions obviously extended more than scale regions (interaction of treatment with region $p<0.01$ for both scales).

Mechanical Manipulations

To examine the effects of extension on lower jaw scale displacement, we compared distances between scales for 11 scale pairs between three treatment groups using one-way MANOVA. Data are shown in Table 7. Our analysis indicates that the three treatment groups differ significantly (Wilks' l=0.00, F=19.68, $p<.001$). However, post hoc comparisons of distances between scale pairs across treatments showed that displacements were not significant for all scales across the three treatments (Table 8). The absolute distances between several pairs of scales did not increase across all treatments due partly to three-dimensional relationships. Specifically, whereas scale–scale distances were measured between the centers of scales, the angle of scales relative to one another and to the plane of stretch was variable. Therefore, if the lower jaw was stretched in one plane/dimension, scales were displaced from their original positions in two dimensions. Interscale distance (i.e. the distance between scale margins, as measured in our behavioral analyses) may increase without a net increase in distance between scale centers.

Distances between pairs GG, AA, AL_5, PP were the only pairs whose scale–scale distance consistently increased across all treatment groups (Table 8). Because the area between posterior chin shields contains additional scales fully or partially hidden in the resting condition, the pairs that provide the best data on single scale–scale relationships across treatment groups used in our study were GG, AA, and AL5. GG and AA have

	Genials		Anterior Chin Shields	
	SW (mm)	INT(mm)	SW(mm)	INT(mm)
Min	0.038 (± .010)	0.0074 (±0.0048)	0.090 (±0.016)	0.012 (±0.010)
Max	0.047 (±.014)	0.030 (±0.017)	0.11 (±0.019)	0.062 (±0.029)
%Change	**24%**	**305%**	**22%**	**416%**
$F_{(1,78)}$	9.99	127.88	18.35	106.00
p	<0.01	<0.01	<0.01	<0.01

Table 6. Average (±S.D.) change in scale widths (SW) and interscale distances (INT) of Genials and Anterior Chin Shields during swallowing events.

scale margins that abut one another in the center, but the scale margins of AL_5 overlap, making accurate measures of interscale distance change impossible.

Histology: *Epidermal changes*

Snake epidermis was described previously from dorsal and ventral body scales (Ficalbi, 1888; Pockrandt, 1931; Maderson, 1964), and even though there are some differences between lower jaw scales and body scales, our description highlights those features that are measurable with the light microscope and that change during extension.

All previous descriptions recognized distinct morphological differences between scale and interscale regions of the epidermis, and it has been relatively well established histochemically that the scale and interscale regions differ in keratin composition (scales contain a thick Oberhäutchen layer with alpha and several beta keratin layers, whereas the interscale regions contain loose alpha keratin and a very thin Oberhäutchen) and secretory capabilities (Alibardi and Thompson, 1999; Banerjee and Mittal 1978; Banerjee and Mittal 1980; Mittal and Singh, 1987a,b). Thus the scale appears to be a well-ordered, rigid structure flexible primarily at its medial and lateral margins (Fig. 12A). The interscale regions (Fig. 12A), which span the space between scale margins, are very different from scales and appear to be highly variable structurally and highly compliant mechanically.

The thickness of the epidermis proved to be difficult to measure across all treatment groups, and because all superficial keratinized layers were difficult to detect and measure with the light microscope, thickness was not used to compare groups quantitatively. Furthermore, in the bumpy, folded regions of interscale epidermis,

	Treatment		
	Rest	Mod	High
$Scale_1$—$Scale_2$	*n*=8	*n*=3	*n*=6
M—G	0.065 (±0.0078)	0.077 (±0.013)	0.085 (±0.011)
G—G	0.076 (±0.013)	0.097 (±0.015)	0.13 (±0.019)
G—A	0.13 (±0.031)	0.11 (±0.019)	0.0.095 (±0.017)
A—A	0.095 (±0.013)	0.15 (±0.023)	0.19 (±0.015)
A—L3	0.15 (± 0.032)	0.12 (±0.016)	0.13 (±0.022)
A—L4	0.13 (±0.016)	0.13 (±0.016)	0.15 (±0.030)
A—L5	0.11 (±0.018)	0.16 (±0.012)	0.19 (±0.032)
P—P	0.13 (±0.021)	0.23 (±0.031)	0.32 (±0.062)
P—L5	0.26 (±0.014)	0.23 (±0.0075)	0.26 (±.026)
P—L6	0.18 (±0.038)	0.20 (±0.036)	0.24 (±0.044)
P—L7	0.11 (±0.17)	0.21 (±0.02)	0.25 (±0.067)

Table 7. Superficial anatomical effects of lower jaw stretching on lower jaw scale spacing. Values are means (±S.D.) of scale—scale distance scaled to jaw length in order to account for size differences among individuals.

		Treatment		
Treatment		Rest	Mod	High
	Rest	**	**GG**, **AA**, **AL5**, **PP**, PL5, PL7	MG, **GG**, GA, **AA**, **AL5**, **PP**, PL6, PL7
	Mod	**GG**, **AA**, **AL5**, **PP**, PL5, PL7	**	**GG, AA, AL5, PP**
	High	MG, **GG**, GA, **AA**, **AL5**, **PP**, PL6, PL7	**GG, AA, AL5, PP**	**

Table 8. Scale—scale interactions differing significantly ($p<.05$) across three treatment groups. Abbreviations are defined in Fig. 3. Distances between scales (4) that differed across all three treatments are in bold.

apparent thickness varied considerably. However, the stratum germinativum was distinguishable across all treatment groups and between scale and interscale regions, and therefore measures of epidermal internuclear spacing (EINS) provided data on the quantifiable changes accompanying extension across treatment groups.

We compared EINS across treatment groups and between scale and interscale regions in the area between the anterior chin shields (AA) using a two-way factorial ANOVA. When comparing treatments using averages of scale and interscale means, there was a significant increase in EINS across treatment groups ($F_{(2, 746)}=67.67$, $p<0.01$). Specifically, compared to the resting condition, EINS was 15% higher ($p<0.01$) in the moderately stretched condition and was 29% higher ($p<0.01$) in the highly stretched condition. Furthermore, EINS was 12% higher in the highly stretched condition than in the moderately stretched condition ($p<0.01$). A significant interaction term indicated that scale and interscale regions differed in EINS between treatments, and these data are shown in Table 9. Specifically, as compared to the resting condition, EINS in the scale region increased by 12% in the moderately stretched condition but only by 3% in the highly stretched condition. Thus, EINS was significantly lower in the highly stretched condition than in the moderately stretched condition. While these results alone are confusing, the difference between the scale and interscale regions' responses were drastically different. In the interscale region, EINS increased by 17% between the unstretched and moderately stretched condition and by an additional 33% between the moderately stretched and highly stretched condition (Table 9). This suggests that the cells of the interscale epidermis are at least partly responsible for taking up some of the strain when the skin is extended, while the cells of the scale regions remain relatively

unaffected by extension.

The morphological changes in the epidermis varied considerably with each treatment. Micrographs of resting (Figs. 12 and 13), moderately stretched (Fig. 14) and highly stretched (Fig.15) conditions illustrate the differences between the scale and intsercale regions with each treatment. The scale epidermis changes relatively little with each treatment as compared to interscale regions. Specifically, the cells of the stratum germinativum in the scale region retain a columnar-cuboidal morphology in all three conditions. SEM micrographs of the surface resting and highly stretched epidermis show that the outer superficial surface of the scale epidermis remains intact and relatively smooth across these two treatments (Fig. 12C, Fig. 15B). The morphology of the interscale epidermis undergoes the most drastic change between treatments. It changes little between the resting and moderately stretched conditions, retaining cuboidal cell shape and the characteristic bumpy nature of the superficial layers (Fig. 13 A,B; Fig. 14B).

Changes occurring in the moderately stretched condition are primarily associated with the unfolding of major skin folds (Fig. 13A-F, Fig. 14B). In contrast, the highly stretched condition differs considerably from the other two conditions. In this condition, the major folds of epidermis flatten, and though the bumpy appearance of the superficial surface is maintained (Fig. 15C,E) the visible cellular layers appear to flatten (Fig. 15C,F). Thus, as EINS increases, there is a marked change in epidermal cell morphology: cells that were cuboidal-round in appearance in the resting and moderately stretched conditions (Fig. 13B, Fig. 14B) take on flattened ovoid shapes when the epidermis is highly stretched (Fig. 15C).

		Treatment		
		Rest	Mod	High
Layer	Scale$_{n=390}$	2.95 (±0.560)*	3.15 (±0.770)	3.05 (±0.60)*
	Interscale$_{n=362}$	3.15 (±0.770)	3.67 (±0.882)	4.91 (±1.30)

Table 9. Comparison of scale and interscale epidermal (stratum germinatival) cell internuclear spacing (in µm) among three treatments. * indicates values that are not significantly different at α=.05. *n*=number of cell pairs sampled.

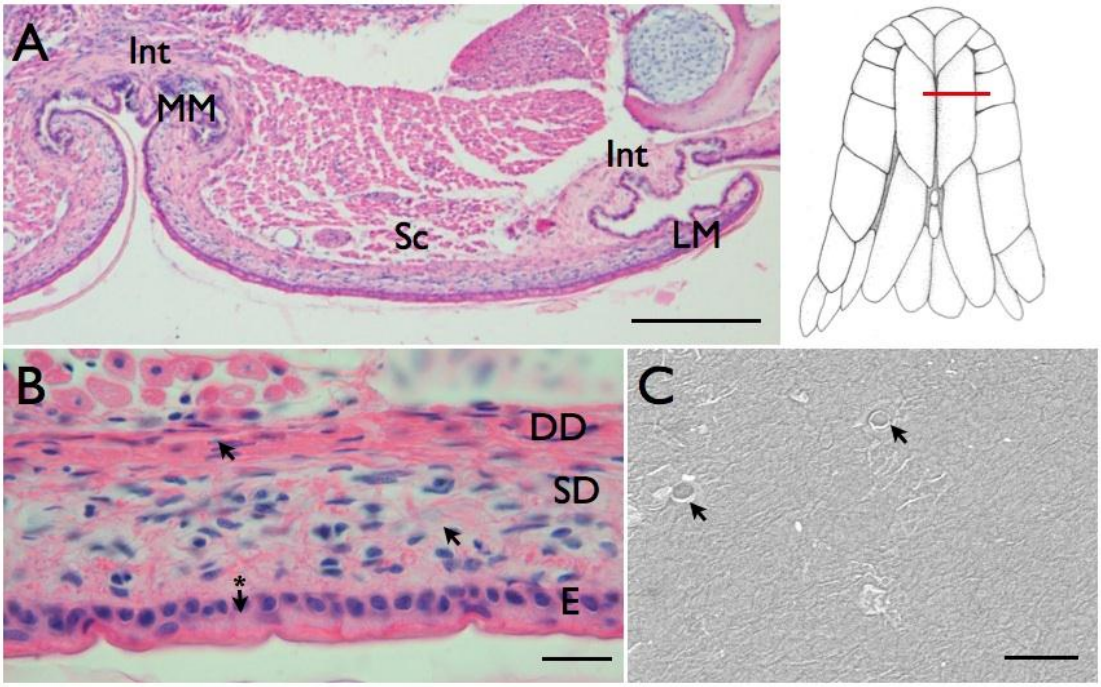

Figure 12. Cross-section of anterior chin shield at the level shown at insert on right. A) H&E stain, scale bar = 100µm. Scale (Sc) and interscale (Int) regions shown as well as lateral (LM) and medial (MM) scale margins. B) H&E stain, scale bar = 10µm. Epidermis (E) is shown and the dermis is divided into superficial (SD) and deep (DD) regions. Arrows without * indicate location of fibroblast nuclei. Arrow with * indicates a nucleus of an epidermal stratum germinativum cell. C) SEM image of outer scale surface, scale bar = 20µm. Arrows indicate external pits in the Oberhäutchen associated with epidermal sense organs (tubercles).

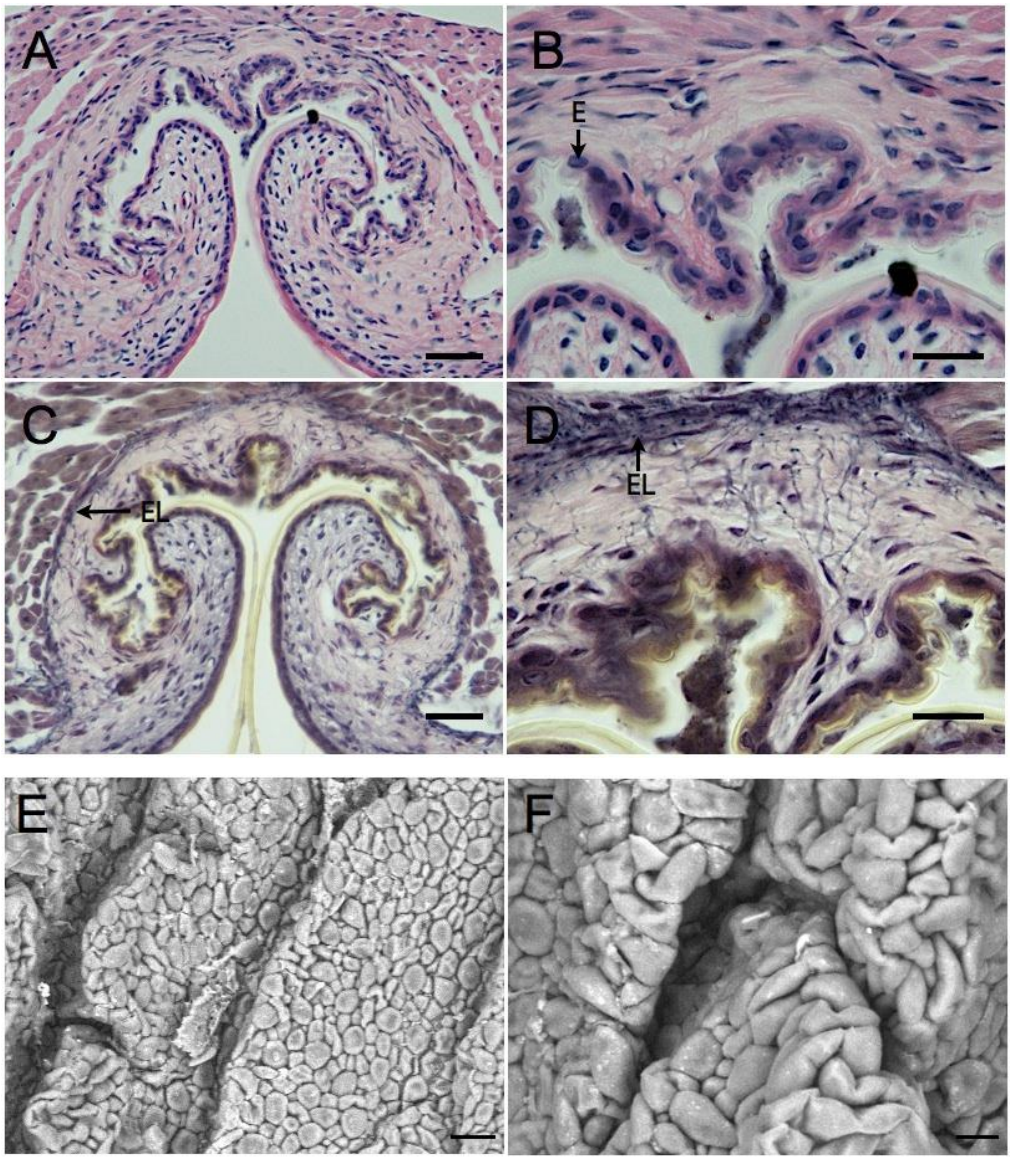

Figure 13. Cross-section of resting interscale skin between the anterior chin shields. A) H&E, scale bar = 20µm. B) H&E, scale bar = 10µm. E-Epidermal stratum germinatival cell nucleus. C) Elastin stain, scale bar = 20 µm. EL-Elastic lamina of the dermis. D) Elastin stain, 1000X, scale bar = 10µm. E) SEM image of outer interscale surface at 500X. Scale bar = 20µm. F) SEM image of outer interscale surface at 1200X. Scale bar = 20µm.

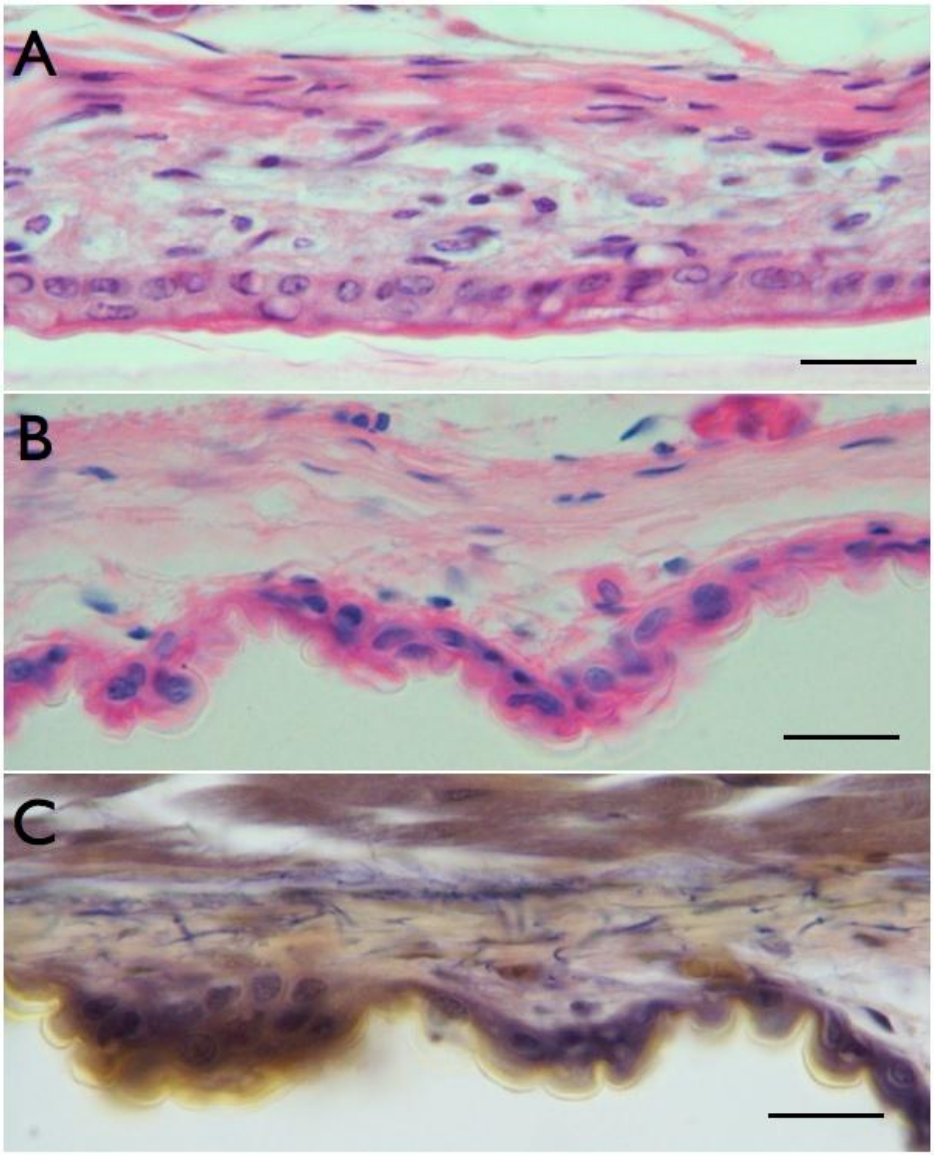

Figure 14. Cross-sections of scale and interscale regions of a moderately stretched specimen. A) Scale region, H&E stain. B) Interscale region, H&E stain. C) Interscale region, elastin stain. In this condition elastin fibers (black) are still oriented in multiple planes. However, many are extending transversely in the plane of stretch. Scale bars = 10μm.

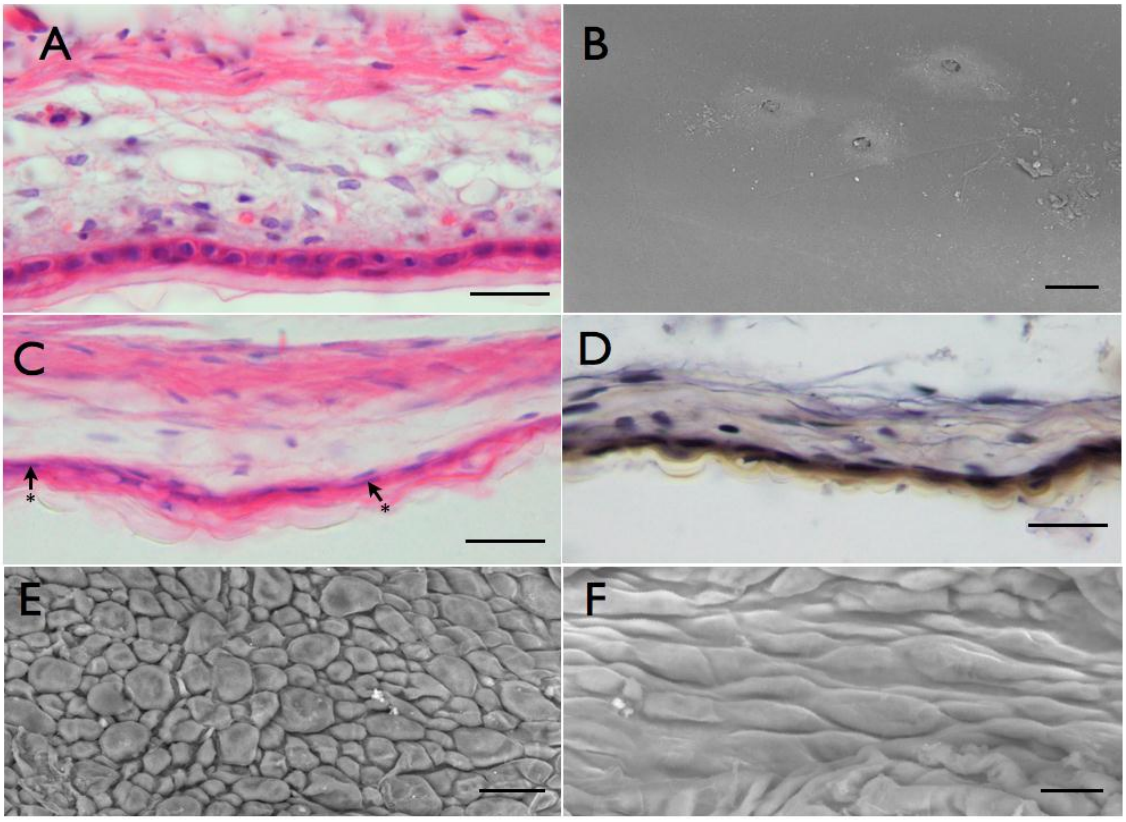
A
B
C
D
E
F

Figure 15. Cross-sections of scale and interscale regions of highly stretched skin. A) Scale region, H&E stain, scale bar = 10µm. B) Scanning electron micrograph (250X) of scale region showing a lack of change in the outer scale surface. Scale bar = 60µm. C) Interscale region, H&E stain, scale bar = 10µm. Arrows indicate cell nuclei in the epidermis. Cells become flattened as the epidermis is stretched. D) Interscale region, elastin stain, scale bar = 10µm. Elastin fibers (black) thin and more laterally oriented as they become further stretched. The elastic lamina is present in this section but is partly out of the focus so that supralaminal fibers can be seen. These superficial fibers extend laterally spanning a region folded in the resting state. E) SEM image of interscale epidermis showing a region that has been unfolded but apparently not stretched because cells are still clustered together and form the minor folds of epidermis. Scale bar = 20µm. F) SEM image of interscale epidermis showing a region that is both completely unfolded and highly stretched. Keratin associated cell surface shows significant deformation in plane of stretch. Scale bar = 10µm.

Histology: Dermal changes

As noted previously by Pockrandt (1937), the dermis of snake skin is composed of two primary layers that are distinguished by both collagen size and distribution as well as elastin content. The superficial dermis is composed of loose collagen fibers that are orthogonally arranged and mesenchymal fibroblasts dominate the cellular content. These regions are more highly vascularized and innervated than the deeper layers, and elastin content is relatively low. The deep layers of the dermis are composed of thicker, transversely oriented, woven bundles of collagen. Elastin is prevalent in the deep dermis and increases with depth to the deepest layers, which are composed (visually) of more than 50% elastin. In the hinge region of the scale collagen fibers course in multiple directions and appear to be more loosely arranged than in the deep dermis under the scale and the interscale dermis. In resting skin the interscale region is devoid of superficial dermis except under some major folds that have a loose arrangement of collagen and the presence of blood vessels. Major folds end at scale bases. The elastin in the interscale region forms a deep elastic lamina from which superficial fibers radiate, and this lamina is continuous with the lamina in the deep dermis of the scale regions.

The thickness of snake skin is difficult to measure because 1) it is divided in to scale and interscale regions, each varying in thickness (Fig. 12A) and 2) because the interscale regions are highly folded in the resting condition (Fig. 13A-F). In regard to the latter, thickness, and therefore cross-sectional area, of the region depends on the 1) amplitude of the folds at a particular stretch condition and 2) the degree to which the dermis can continue to stretch once the folds flatten.

We first compared average fold amplitude from two scale pairs (AA, and AL5) across the three treatment groups using a two-way factorial ANOVA. Values for average fold amplitude for each scale pair and across three treatments are shown in Table 10. Our ANOVA indicated that treatment groups ($F_{(1,188)}$=41.97 , p<0.01) and regions ($F_{(1,188)}$=19.736, p<0.01) differed significantly in fold amplitude. However, there was no significant interaction between treatment and region (AA vs. AL5) sampled ($F_{(2,188)}$=1.014, p=0.365), and, therefore, interscale regions, though different in absolute fold amplitude, respond to stretch by similar decreases in fold amplitude. Post hoc tests revealed fold amplitude decreased from the resting condition by 35% in the moderately stretched condition (p<0.01) and by 65% in the highly stretched condition (p<0.01). Fold amplitude was 46% lower in the highly stretched condition than it was in the moderately stretched condition (p<0.01). Thus, as our epidermal and dermal records indicate, and has been assumed for over a century (Ficalbi, 1888), the extension of snake skin primarily involves the unfolding of the interscale region.

Because the superficial dermis varied in thickness and was non-uniform, we measured the thickness only of the deep dermis across three treatment groups, and compared treatments using a one-way ANOVA. Values of dermal thicknesses among three treatments are summarized in Table 11. Our one-way ANOVA results showed that the average thickness of the deep dermis varied across treatment groups ($F_{(2,183)}$=8.09, p<0.01). Post hoc analyses indicated that the average deep dermal thickness in the moderately stretched condition was significantly less than the resting condition (p<0.05). However, the resting condition and highly stretched condition did not differ significantly (p=0.11) and the highly stretched condition was significantly thicker (<0.01) than the

		Treatment		
		Rest	Mod	High
Region	$AA_{n=30}$	15.9 (±9.11)	9.80 (±6.13)	6.34 (±4.09)
	$AL_{n=30}$	11.1 (±4.44)	7.67 (±3.78)	10.53 (±7.65)
$Total_{n=60}$		**13.5 (±7.51)**	**8.76 (±5.20)**	**4.70 (±3.47)**

Table 10. Differences in average interscale fold amplitude (in mm) among three treatment groups. Values shown are from two interscale regions sampled (AA and AL). Abbreviations defined in text. *n*=number of observations.

moderately stretched condition. It is important to note that every effort was made to measure the dermis in the same relative location along the scale between treatments, and thus the result that the deep dermal thickness was higher in the scale region is puzzling.

We used average internuclear spacing of fibroblasts in the dermis (DINS) to determine the degree to which this part of the skin changes with stretch treatment. We first sought to determine whether and how the dermal strata in the scale regions responded to stretch. Therefore, we used a two-way factorial ANOVA and tested the interaction between treatment and dermal strata. Our ANOVA showed that average DINS differed between treatment groups ($F_{(2, 114)}$=38.05 , p<0.001) and indicated a significant interaction between treatment and dermal stratum ($F_{(2,1144)}$=12.42, p<0.01; see Table 9). In the superficial dermis, DINS increases by only 3% in the moderately stretched condition and by only 16% in the highly stretched condition. Furthermore, DINS in the highly stretched condition was only 12% higher than the moderately stretched condition. In contrast, DINS in the deep dermis increased by 35% in the moderately stretched treatment and by 57% in the highly stretched condition. These results suggest that the deep dermis exhibits a much more marked response to stretch than the superficial dermis.

The interscale dermis is continuous with the deep dermis of the scale region and is similar in its morphology. Therefore we compared DINS of interscale dermis between treatment groups using a one-way ANOVA. Our analysis revealed a significant difference across treatment groups ($F_{(2,758)}$=34.01, p<0.001). Post hoc analyses indicated that DINS increased significantly by 30% between the resting and moderately stretched condition (p<0.01) and by 43% between the resting and highly stretched conditions. Similarly, DINS increased by 10% between the moderately stretched and highly stretched

conditions (p<0.01). We did not test for differences between scale and interscale regions in this variable. However, given that the deep dermis is continuous across scale and interscale regions, DINS likely increases similarly in each during extension.

Elastin

Pockrandt (1937) first described the distribution of elastin in the deep dermis of snake body skin. While some studies indicate that elastin in mammal skin makes up a mere 4% by mass of the total dermal content (Gibson and Kenedi, 1970), its composition through the depth of the dermis is variable. In the resting condition of snake skin, the deepest layers of the dermis are abundant in elastin, forming a dermal *elastic lamina* from which fibers radiate superficially through the deep dermis and presumably attach to collagen in the extracellular matrix and basal lamina of the epidermis (Fig. 13C,D). The elastic layer courses through the deep dermis of the scale as well as the interscale regions and elastic fibers extend from the deep layer superficially to the hinge region of the scale (*inner scale surface*) and to the base of folds in the dermis. In the scale region superficial excursions of elastin into the superficial dermis are relatively rare, and most of the elastin is closely associated with the woven collagen fibers of the deep dermis.

The elastin fibers radiating out of the elastic lamina are presumably anchored to the basal lamina (basement membrane) of the interscale epidermis at particular regions (i.e., the base of folds). In the moderately stretched condition (Fig. 14C) as the folds flatten, the dermal folds of interscale skin begin to unfold and the elastic lamina begins to stretch in the transverse plane. Meanwhile, the fibers radiating from this layer begin to stretch as the anchoring sites on the elastic lamina move further away from one another.

	Treatment		
	Rest	Mod	High
Thickness $_{n=186}$	11.19 (±4.62)	9.75 (±2.78)	12.37 (± 4.22)
DINS$_{n=761}$	7.29 (±3.46)	9.51 (±4.36)	10.45 (±4.02)

Table 11. Differences in average deep dermal thickness and fibroblast internuclear spacing (DINS) among three treatment groups. Samples collected from both scale and interscale regions. DINS was significantly different across all treatments at *a*=.05. For Thickness, lines connect group means that were significantly different at *a*=.05. *n*=number of samples.

		Treatment		
		Rest	Mod	High
Layer	Superficial$_{n=759}$	7.18 (±2.90)	7.44 (±2.82)	8.35 (±3.15)
	Deep$_{n=391}$	6.88 (±3.89)	9.29 (±4.37)	10.81 (±4.50)

Table 12. Dermal effects at the level of the scale: Comparison of fibroblast internuclear spacing (in μm) in superficial and deep layers of scale dermis across three treatment groups. *n*=number of fibroblast pairs measured.

In the highly stretched condition, the folds have flattened, and superficial fibers become thinner and oriented transversely (15D). In this highly extended state, the elastic lamina and the fibers that course from it should be at lowest entropy. Therefore, when the load is released, the elastic lamina and the radiating fibers should both act to return scales to their resting position and return folds of hinge and interscale epidermis to their resting condition.

Nerve supply

The scales of the lower jaw are innervated by the mandibular branch of the trigeminal nerve (V_3, Auen and Langebartel, 1977), and scales we examined were innervated by at least three divisions of this nerve. The posterior chin shields receive innervation from both a small branch that exits a foramen on the medial surface of the compound bone posteriorly, as well as a branch exiting the medial side of the mandible at the level of the intramandibular joint. The anterior chin shields receive innervation only from the latter branch, which is extensively branched at the level of the anterior chin shield and courses anteriorly to finally terminate in the genial scales. The genials, in addition to being innervated by this branch, receive additional innervation from a branch that supplies all other labials. This latter branch exits the mental foramen on the lateral surface of the dentary and sends fibers anteriorly into the mental scale as well as posteriorly to supply the infralabials (Fig.16A).

Given the degree to which the lower jaw and skin extend during stretching, very few of these nerve fibers are highly convoluted in the resting condition. However, most nerves are arranged longitudinally. One peculiarity of nerve distribution is that at least

one major branch innervates several scales and must cross scales as it courses anteriorly. The problem is evident when the lower jaw is stretched (Fig. 16B), and the arrangement can only be explained by the fact that the nerves must only be attached to scales at points that would minimize the absolute distance between scales. As our mechanical manipulations showed, the distance between scales is least at the anterior and posterior borders (often imbricating) of adjacent scales. In order for V_3 to course between an anterior chin shield and a genial, it either travels within the dermis of the interscale region between these two scales or bypasses the interscale region and enters the base of the scale separately.

Serial sections of the junction between the anterior chin shield and the adjacent genial confirm this relationship. As seen in Fig. 11, V_3 courses just below the dermis of the scale, and sending fibers superficially to the anterior chin shield (and thus periodically crossing the dermis) at certain points along this scale. When the nerve moves toward the genials it courses close to the dermis at the junction between the scales and eventually crosses the dermis into the base of the scale. Therefore, the major portion of the nerve is "anchored" only at its anterior limit.

In the stretched dermis (Fig. 16B) there is a gross reorientation of fibers from longitudinal to transverse, but exactly whether and how peripheral branches of nerves move relative to one another was difficult to determine. It is likely, though, based on the relationship of the nerves to the scales (Fig. 17), that reorientation can occur without a great deal of extension. Because the nerves are not highly convoluted in the resting condition, it seems as though more reorientation occurs meaning gross arrangement plays an important role in the extensibility of the neural network innervating the skin.

A

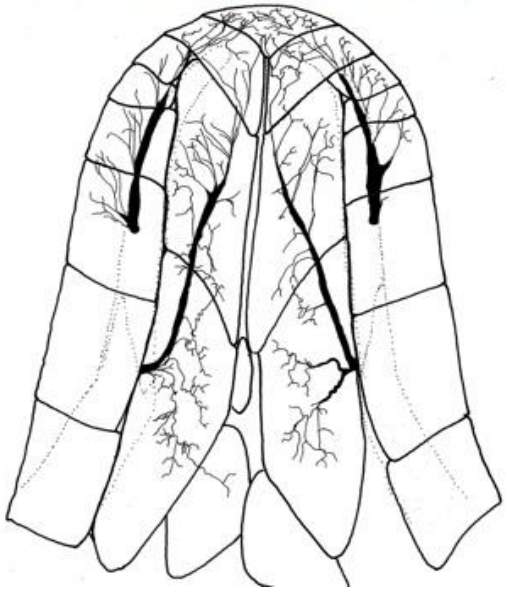

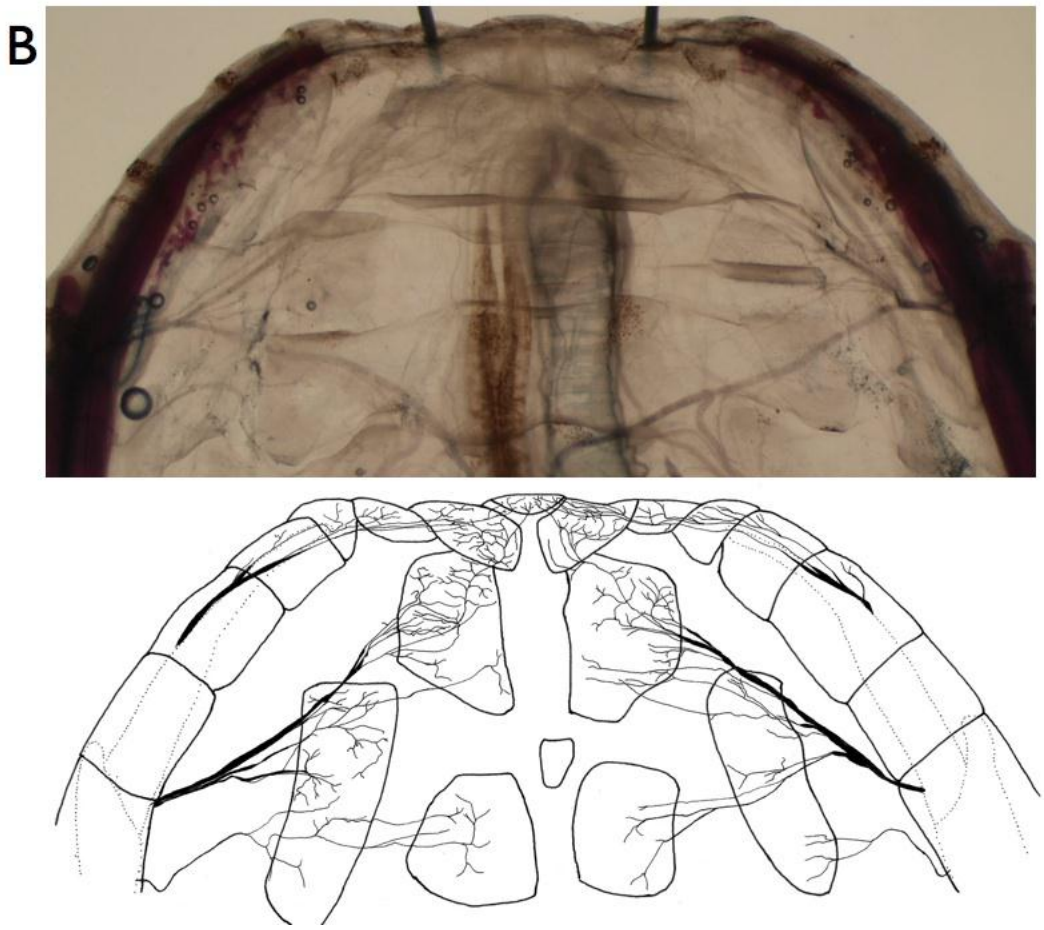

Figure 16. Patterns of scale innervation. A. Resting. B. Stretched. In each, the upper picture is a cleared and stained specimen and the lower is a ink tracing of nerves and scale outlines. Dotted lines represent the mandibles.

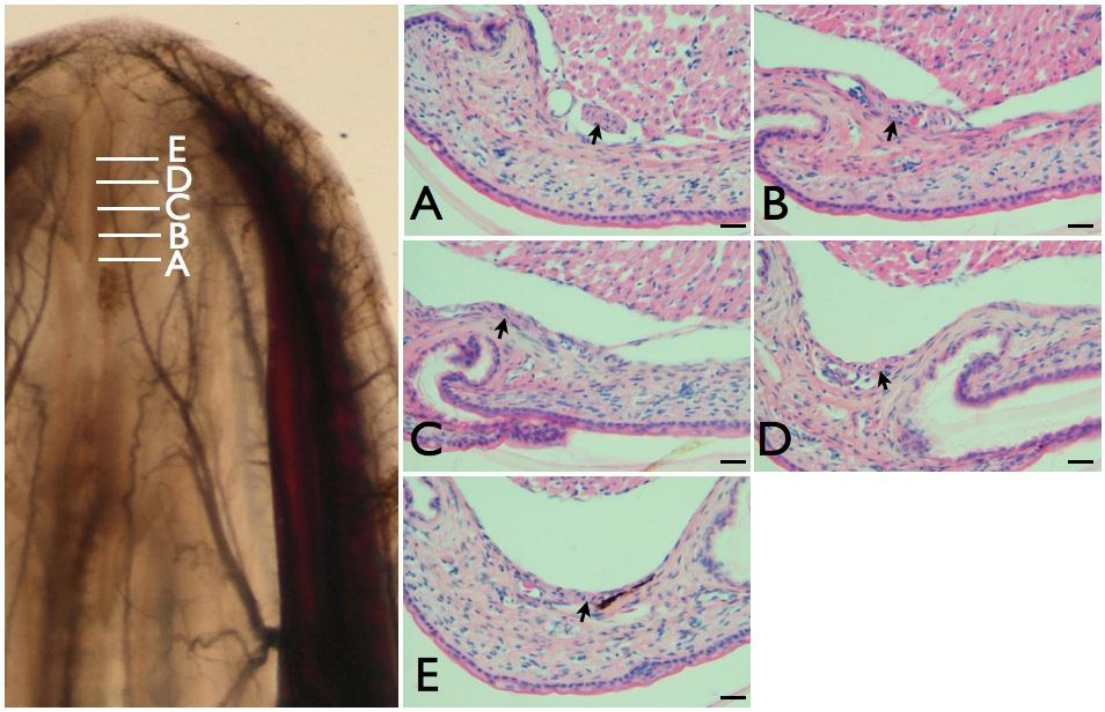

Figure 17. Serial cross sections (A-E, posterior to anterior) through junction between anterior chin shield and genial scales showing course and entry of nerve (arrow) and adjacent blood vessel into base of genial scale. Scale bars=10µm.

DISCUSSION

Many snakes have the ability to ingest remarkably large prey, and it has long been recognized that one of the primary determinants of gape size in snakes is the extensibility of the intermandibular connective tissues (Gans, 1961; Arnold, 1983; Cundall and Greene, 2000). Understanding the structure and behavior of the basic materials linking the tips of the mandibles is important to understanding how gape size evolved within snakes. Similarly, understanding how these materials behave in the living organism informs our perception of their relative importance.

Previous analyses of the performance of the feeding apparatus in watersnakes have used measures of skeletal or external head features that are easy to record and correlate to gape size (Hampton, 2011; Herrel et al., 2008; Queral-Regil and King, 1998; Vincent et al., 2006a; Vincent et al., 2006b; Vincent et al., 2007). Although lengths of skeletal elements such as the quadrate and mandible have high positive correlations to gape, gape size in snakes results not only from skeletal features (or the external features that overlay them) but also from the degree to which soft tissues can stretch. While field experiments have shown that "gape" (i.e., cross-sectional area) calculated from head dimensions alone deviated from prey cross-sectional area, and while it has been well-established that intermandibular extensibility is key to snake gape, in only a single recent study by Vincent et al. (2006b) was intermandibular distance measured. The results showed that intermandibular distance was significantly positively correlated to prey width, but unfortunately no explanation was provided of how intermandibular separation occurred. Finally, studies of snake feeding performance that have used ingestion rate as a

measure have generally used prey well below the maximum size the snake could swallow. As a result, we know little about the real gape potential of most snakes.

During feeding (intraoral prey transport: Cundall and Greene, 2000) the mandibles of watersnakes separated slightly beyond 7X their distance at rest, and the process took more than 20 min in some cases. Therefore, ingesting large prey involves extending tissues over relatively long periods of time. Our mechanical tests corroborate partially corroborate this relationship: intermittent increases in strain, allowed the mandibles to separate to 10X their resting distance without failure. Few anatomical structures in vertebrates have this capability (Brainerd, 1994; Vogel. 2003; Wainwright et al., 1976;). We analyzed some of the structural results of extension in the skin to refine hypotheses the mechanism of tissue extensibility. Recent studies of snake skin have dealt with its mechanical properties in the context of locomotion (Berthe et al., 2009; Jayne, 1988; Klein et al., 2010) and macrostomy (Rivera et al., 2005). Even though it has long been noted that snake interscale skin stretches more than scale regions, to date, only two studies (Pockrandt, 1937, Savitzky et al., 2004) have given serious attention to the anatomical basis of the ability of skin to stretch. Savitzky et al. (2004) showed that there was a correlation between dorsal scale row arrangement and macrostomy, or the ability of the skin to stretch in the circumferential axis. They suggested that arrangements of body scales and interscale regions correlated with the ability to stretch in the circumferential axis. Thus, the extensibility of skin as a whole was dependent on the arrangement of scale rows relative to the long axis of the body. Savitzky et al. (2004) also suggested that the ability of the skin to recover from a stretched condition was aided by elastin networks that spanned the interscale region. Our histological data shows that the ability of folded

interscale skin to unfold during stretch and refold when relaxed rests in the structure, composition and behavior of the deep dermis (*stratum compactum*).

A Model of Snake Skin Extensibility

The resting condition is distinguished from all others by folding of the interscale skin (Fig. 18A). Histologically, the major folds are produced by dermal ridges which are overlain by a very thin interscale epidermis. At rest the cells of interscale epidermis take on a variety of shapes, but the predominant shape of the living cells (i.e., the stratum germinativum and the *cellules à mamelon*) is cuboidal. Due to the extensive folding the cells are packed closely together and, in combination with the bizarre shapes of the *cellules à mamelon*, form minor folds in the surface. The collagen fibers of the deep dermis are thick and are parallel/interwoven in the interscale and scale regions and both parallel/interwoven and orthogonal in the hinge regions. The deepest layer of the dermis is essentially an elastic lamina from which elastin fibers radiate transversely, orthogonally and superficially at the base of folds.

The moderately stretched condition (Fig. 18B) is characterized primarily by an unfolding of the major folds of interscale skin. As the region unfolds, cells in the epidermis become less packed, and this is accompanied by a slight increase in the distance between nuclei. However, cell shape does not change drastically and the minor folds of the surface are preserved. The dermis responds to unfolding in a slightly more dramatic way—the collagen fibers tend to be reoriented in the plane of extension and the elastin fibers begin to stretch as the basal lamina of the epidermis and the elastic lamina of the dermis extend. Fibroblasts in the dermis are spaced farther apart, indicating that the

extracellular matrix is undergoing notable change. This condition can be described by slight unfolding of the epidermis and flattening of the dermis.

The highly stretched condition (Fig. 18C) is characterized by further unfolding and (at least in some cases) stretching of the interscale skin. The major folds disappear and many of the minor folds decrease in amplitude. The latter is associated with changes in cell shape as the cells of the interscale epidermis become flattened. The distance between nuclei of cells in this layer also increases which suggests that deformations/strains are occurring at the cellular level. The dermis responds to continued extension by stretching. Once the folds flatten, collagen is no longer recruited from superficial layers of interscale dermis (i.e., dermal folds), and therefore the region is stretched. Collagen fibers are reoriented in the plane of stretch. The deep dermis increased this condition. Although it is possible that this was artifact of preparation, it is also possible that the slow increase in extension allowed for collagen fibers to slip relative to one another, decreasing the number of cross-links and increasing the amount of interfibrillar space. Elastin fibers continue to stretch (to the point where some are difficult to identify with the light microscope), but seem to still maintain their association with the basal lamina of the epidermis and the elastic lamina of the dermis. Therefore, the highly stretched condition can be characterized by a further stretching of the interscale and deep dermis.

How, then, does the skin return to its resting folded condition? Based on our histological data, it is clear that a mechanism of passive elastic recoil could account for much of the refolding of the interscale epidermis. In the unstretched condition, fibers are anchored at sites on the basal lamina of the epidermis preferentially in the "valleys"

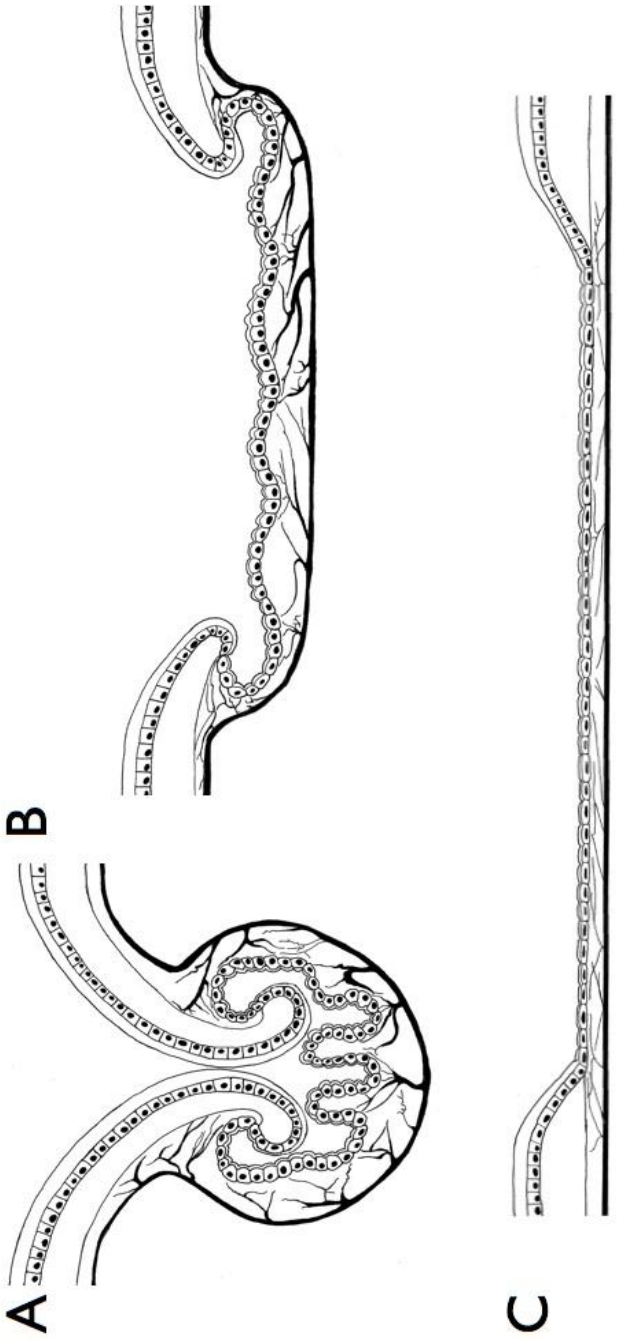
A
B
C

Figure 18. Model of skin stretching. A. Unstretched. B. Moderately stretched. C. Highly stretched. The outer strata and keratinized layers of the epidermis are not distinguished and appear as a single layer outside of the stratum germinativum.

between folds of the skin and occasionally to the adjacent and opposite walls of folds (Fig.19A).

Fibers either course directly to the elastic lamina of the dermis or converge with other fibers at trunks, which then meet the elastic lamina, but in either case, elastin is attached to the epidermal basal lamina and to the dermal elastic lamina (Fig. 19B). When the folded regions are stretched, the distance between the anchoring sites increases and the elastin polymers stretch.

Refolding of the interscale skin occurs when the load is released and elastin is permitted to recoil. The attachment sites on the elastic lamina come closer together bringing the dermis of the "valleys" closer together. At the same time, the depth of the "valleys" is recovered by the recoil of elastin between the basal lamina and the elastic lamina.

The deformation of the dermis is dominated by reorganization of the extracellular matrix and by extension of the molecular rubber that composes a large portion of its deep layer. Under a relatively high strain rate, the reorientation of collagen fibers would occur, but tension would rise more quickly as collagen fibers would remain cross-linked and fairly rigid. Under slow strain rates, which may reduce cross-linking, fibers presumably reorient and slide relative to one another increasing the potential for irreversible creep (Craig et. al., 1987). Return from this state therefore requires the recovery of the stretched elastin, which remains anchored at the basal lamina and the elastic lamina.

At higher strain rates, it is unlikely that the epidermis would do more than unfold since tension would rise primarily in the underlying dermis before strain was imposed on the cells of the epidermis. However, under low strain rates (as used in our study and

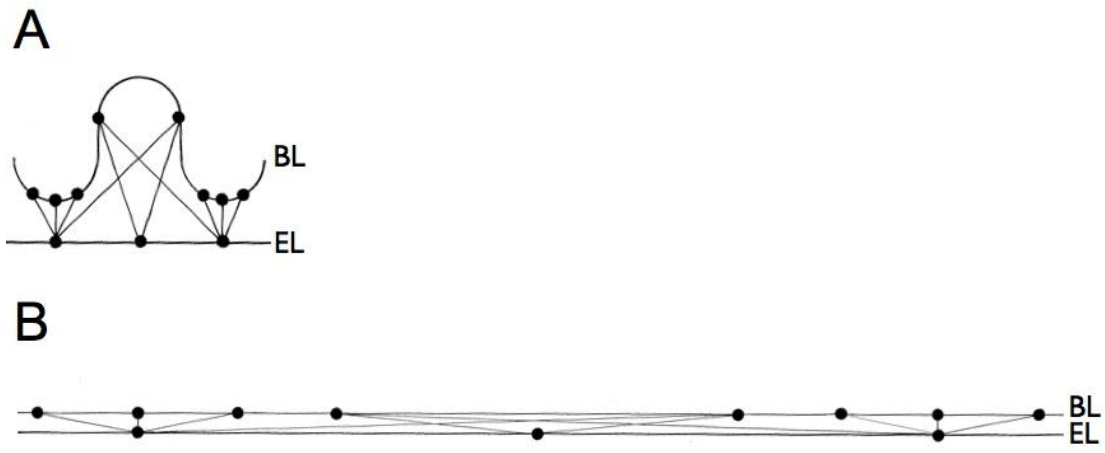

Figure 19. Model of unfolding and refolding mechanism based on histological data. A. Resting condition. B. Stretched Condition. Elastin fibers extend from the elastic lamina (EL) of the deep dermis and are presumably anchored to points (●) along the basal lamina (BL) of the epidermis.

during feeding by the snakes), the folds flatten and cells of the epidermis would stretch slowly and become flattened. In order for cells to remain in their location, membrane proteins of the basilateral surfaces might have to rearrange to allow the basal surface to move with the basal lamina (basement membrane) and the lateral surface to reduce with its attachment to neighboring cells. At high levels of extension, the soft alpha keratin of the superficial layers unfolds and subsequently refolds when the load is reduced. Return from the highly extended state would require further reorganization at the basolateral surfaces of cells—probably until the resting state is fully recovered. The types of changes seen in the epidermis are not well documented in the literature and require further investigation using ultrastructural techniques.

The architecture of squamate skin contains the structural potential to evolve from a movable armor sufficient for locomotion (e.g., lizards and amphisbaenians) to an extensible armor well suited for macrostomy (snakes). This unique integument is not the only limiting feature of intermandibular extensibility, but it is integrated with the network of deeper tissues linking the mandibles and thus plays a critical role. Furthermore, its response to mechanical stress (stretching) exhibits features that may be shared among other intermandibular soft tissues. Whether other highly extensible vertebrate tissues share the passive intra- and extracellular elastic mechanisms that have evolved in snakes to recover their resting state remains to be seen.

CHAPTER 4

Extensibility of Muscle

SUMMARY PARAGRAPH

Many snakes possess the phenomenal ability to swallow extremely large prey whole. During swallowing, the tips of the mandibles can separate more than 700% of their resting distance, and under these conditions, the muscles connecting their distal tips are highly stretched, but subsequently recover normal function. Recovery from extreme extension requires contributions from extracellular connective tissues, intracellular elastic elements, and spontaneous contraction. In the highly stretched condition, sarcomere length (SL) increases 200% its resting value (SL_o) or more, and actin and myosin filaments no longer overlap. Myofibrils fall out of register and triad organisation is disrupted. Recovery requires recoil of intracellular titin filaments, but must also involve additional elastic cytoskeletal components responsible for realigning myofibrils. Following passive recovery, SLs were 82% of SL_0, creating a region of double-overlapping actin filaments, a condition requiring contraction in the absence of stimulation. Stretch of whole muscles exceeded that of sarcomeres due to folded terminal tendon fibrils and abundant endomysial elastin allowing independent movement among muscle fibres. Snake intermandibular muscles thus provide a unique model of how the basic components of vertebrate skeletal muscle can be modified at various levels to permit extreme extensibility.

MAIN TEXT

Skeletal muscles have passive elastic properties resulting from a combination of components: titin filaments within the sarcomeres, an internal cytoskeletal network, and collagen and elastin fibres in extracellular connective tissues (Wang et al., 1993). The latter come into play at long lengths and determine how far a muscle can stretch without breaking (Dulhunty and Franzini-Armstrong, 1975). Extension of skeletal muscles *in vivo* is usually limited to lengths that lie within the range of overlap of actin and myosin filaments. However, a striking exception to this generalisation is found in a bilaterally paired, transversely oriented muscle connecting the unfused mandibular tips of colubroid snakes—the *M. intermandibularis anterior*, *pars anterior* (MIAA). During swallowing events, the distance between the mandibular tips can increase to 700% or more of resting distance, and each MIAA (left and right) may extend to 300% or more of its resting length and subsequently recover by currently undefined properties of passive elastic elements.

Analysis of laboratory video records of northern watersnakes (*Nerodia sipedon*) swallowing fishes (*Notemigonus crysoleucas*, *Oncorhynchus mykiss*, *Pimephales promelas*, *Salmo trutta*, and *Salvelinus fontinalis*) showed that the distance between the tips of the mandibles reached its maximum value—which ranged from 250–770% of resting distance (Fig. 20a,b). Intermandibular distance was positively correlated (r^2=0.35) with ingestion ratio, the ratio of prey cross-sectional area to snake gape cross-sectional area, suggesting that snakes that ingest relatively large prey tend to exhibit greater extensibility of the intermandibular soft tissues (e.g., muscle; Fig. 20c,d).

We compared the anatomy and ultrastructure of the MIAA in resting, stretched, and recovered lower jaw apparatuses from size-matched adult watersnakes. Lengths of

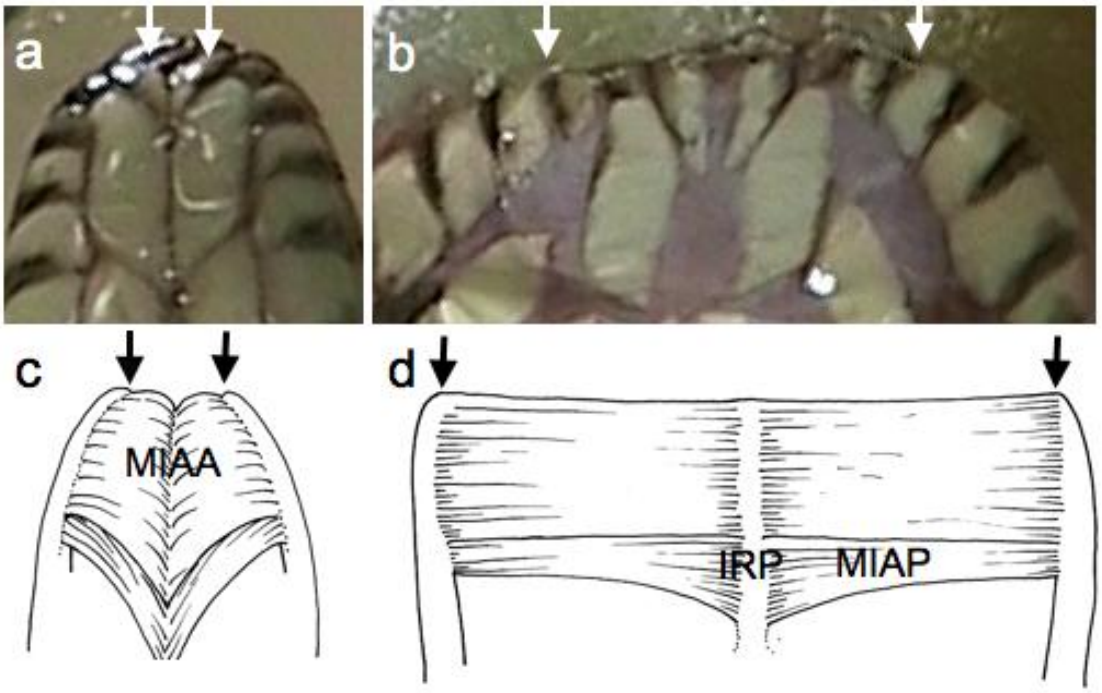

Figure 20. a,b) Video fields taken from a recording of an adult watersnake (*Nerodia sipedon*) ingesting a trout. a) Resting; white arrows indicate the approximate locations of the mandibular tips. b) Stretched; white arrows as in A. The stretched intermandibular distance is ~650% resting distance. c,d) Illustrations showing the relationships of intermandibular muscles to the madibles (origin) and interramal pad (midline insertion) in the resting (c) and stretched (d) conditions. Black arrows indicate the locations of the mandibular tips. The stretched intermandibular distance is ~600% resting distance. IRP, interamal pad; MIAA, *M. intermandibularis anterior, pars anterior*; MIAP, *M. intermandibularis anterior, pars posterior*.

stretched muscles were 270% those of resting specimens, but average sarcomere length (SL) for stretched muscle fibres was only ~210% of resting length (SL_0) (Table 13). In stretched fibres, actin and myosin filaments no longer overlapped, creating a gap region spanned by superthin (titin) filaments (McNeil and Hoyle, 1967; Locker and Leet, 1975; Horowitz et al., 1986; Salviati et al., 1990; Table 13, Fig. 21a,b). The average Z-line to A-band distance was 1.9±0.33μm, presumably within the range of titin extension (Salviati et al., 1990). Distances between Z-lines of adjacent myofibrils was significantly greater in stretched fibres ($p<.01$; Table 1, Fig. 21f,g), with concomitant distortion of some triads (Fig. 21i,k).

In recovered fibres, the gap region disappeared and myofilament overlap was reestablished (Fig. 21c). However, average SL was significantly shorter than in resting fibres ($p<.01$, Table 13), and actin filaments from adjacent hemi-sarcomeres overlapped in the middle of the sarcomere (Fig. 21c,d). There were no damaged "popped sarcomeres," as commonly seen in skeletal muscle that has been stimulated at high levels of extension (Locker and Leet, 1975). Alignment of both Z-lines (Fig. 21h) and triads (Fig. 21k) is restored in recovered fibres, supporting the existence of elastic elements in both myofibrillar and cytoskeletal architecture.

At a minimum, two components must be involved in length recovery. Initial shortening depends on passive elastic properties, as there is no myofilament overlap to facilitate active contraction (Fig. 21b,e). Current models of titin function, generated primarily from studies of the isolated protein (Kellermayer et al., 1997; Linke et al., 1998; Trombitas et al., 1998), show it can extend reversibly to lengths of 1.5–4μm (Linke et al., 1998). Until now there has been no evidence of it doing so *in vivo* under normal

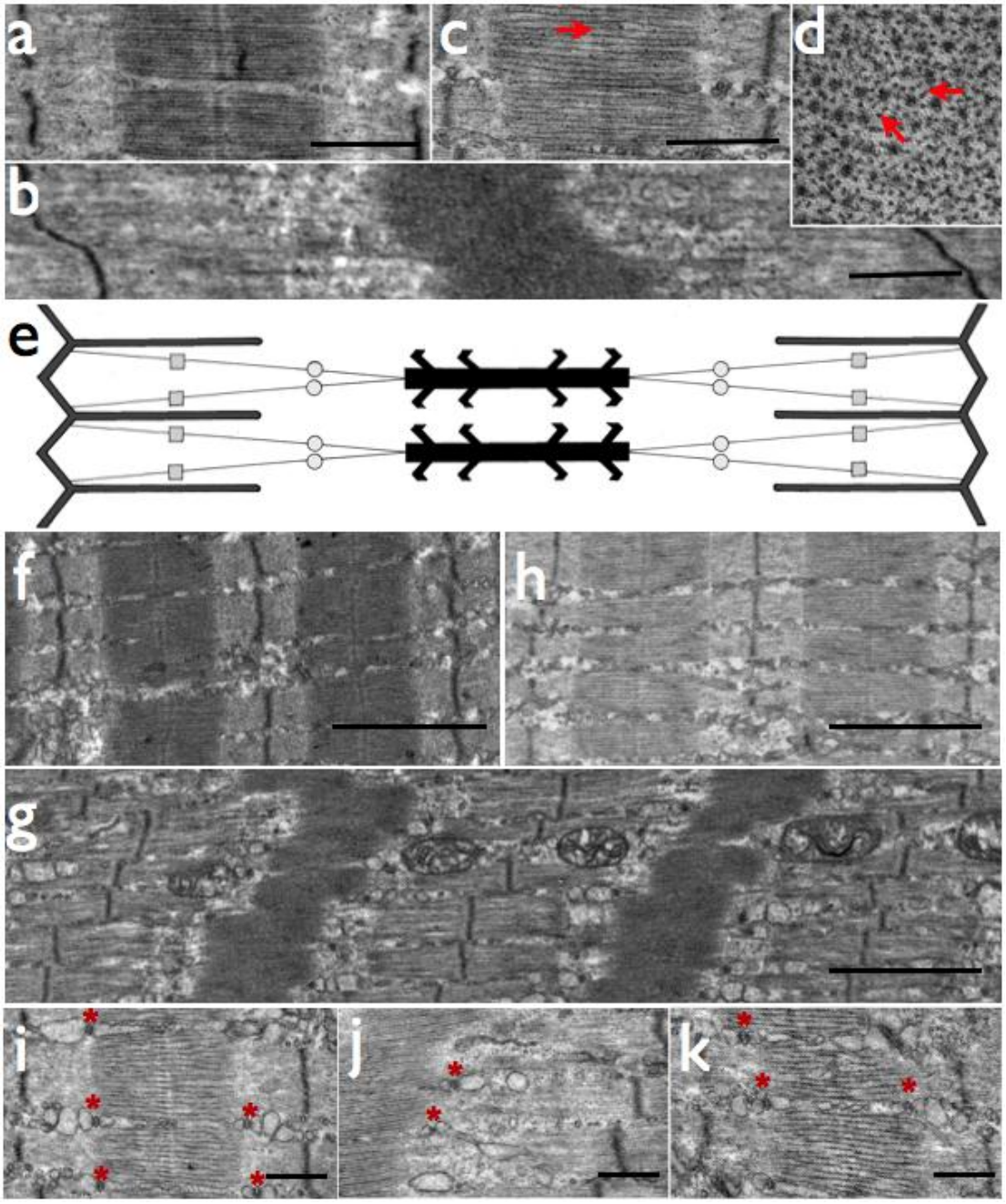
a
c
d
b
e
f
h
g
i
j
k

Figure 21. TEM micrographs of resting, stretched, and recovered intermandibular muscles of watersnakes (*Nerodia sipedon*). a–c) Longitudinal sections of fibres in the resting (a), stretched (b), and recovered (c) condition. Arrows indicate areas of double overlapping actin filaments in the middle of sarcomeres. Scale bars = 0.5μm. d) Cross-section of a recovered fibre showing double-overlap of thin filaments at mid-sarcomere (arrows). e) Two-dimensional model of highly stretched sarcomere, incorporating a model for titin. □ represents the N2A region and ○ represents the border of the PVEK and distal tandem Ig segments. For simplicity, only two of the six titins for each half sarcomere are shown. Titin may provide positional stability of myofilaments at high degrees of stretch: refolding/recoiling of the molecule guides thin filaments back into position. However, double overlap seen in recovered muscle presumably requires active contraction. f–h) Longitudinal sections of fibres at lower magnification showing Z-line relationship between adjacent myofibrils in resting (f), stretched (g), and recovered (h) fibres. Scale bars = 2.0μm. As seen in g, the Z-lines become staggered as a result of stretching, but recover after loads are released (h). Longitudinal sections of resting (i), stretched (j) and recovered (k) fibres showing alignment of triads (*) with the end of the A-band. In the stretched condition, the triads remain close to the A-band but their aligment is not uniform. Furthermore, there is some distortion of the terminal and intermediate cisternae. Scale bar = 0.5μm.

	Resting	Stretched	Recovered
Total Muscle Length (μm)	2.6±0.061 (n=2)	7.0±0.41 (n=2)	2.7±0.14 (n=2)
Sarcomere Length (μm)	2.63±0.02 (n=189)	5.49±0.87 (n=119)	2.15±0.21 (n=63)
Z-line –A Band (μm)	0.55±0.04 (n=30)	1.92±0.33 (n=30)	0.32±0.07 (n=30)
Gap (μm)	0	0.82±0.15 (n=25)	0
$Z\text{-line}_{fibre1}$–$Z\text{-line}_{fibre2}$ (μm)	0.13±0.11 (n=100)	0.46±0.37 (n=100)	0.09±0.12 (n=100)

Table 13. Summary of anatomical and ultrastructural data for resting, stretched, and recovered snake MIAA muscles. All values are means±standard deviations. For total muscle length, means represent measurements from both right and left sides of same individual.

physiological conditions. The initial sarcomere recoil in the MIAA offers *in vivo* confirmation of titin's role but does not explain the recovery of myofibrillar and membrane arrangements. These might be explained by a second set of elastic cytoskeletal proteins extending between myofibrils (Pierobon-Bormioli, 1981; Tokuyasu et al., 1983; Wang and Ramirez-Mitchell, 1983) and by default membrane realignment occurring as myofibrils realign themselves (Magid and Law, 1985).

The second event, facilitated by the double overlap of actin filaments (Fig. 21c,d), requires active contraction (Dulhunty and Franzini-Armstrong, 1975), suggesting that final length recovery depends on muscle activation. Since the recovery achieved in the MIAA occurred in the absence of direct stimulation, it is possible that full recovery was achieved by the biomechanical phenomenon of stepwise shortening (Granzier and Pollack, 1985; Nagornyak and Pollack, 2005; Pollack et al., 2005), a well-documented process of passive recovery that is currently poorly understood from both ultrastructural and molecular perspectives. If stepwise shortening accounts for the recovered condition we observe (Fig. 21c,d), then there are certainly roles for both elastic recoil of superthin filaments and cross-bridge cycling once myofilament overlap has been re-established. If this is the case, these two distinct phases should be observed in the mechanical behaviour of fibres recovering from high levels of extension.

The relative increase in SL is less than that of the whole muscle after stretching (Table 13). A similar occurrence was reported previously in the tongue retractor muscle of an agamid lizard (*Pogona vitticeps*), in which SLs increased by only 120% for a total muscle extension of 150% (Herrell et al., 2002). This arises from a third component of stretching involving rearrangement of the connective tissues surrounding muscle fibres

(Borg and Caulfield, 1980; Rowe, 1981; Purslow, 1989), allowing independent slippage of the fibres relative to each other. Cross-sections of stretched whole-muscle fibres completely lack the polygonal shape found in the resting fibres (Fig. 22a) and are spaced further apart (Fig. 22b). This arrangement, a product of changes occurring in the intracellular environment, also requires physiological adaptation of the extracellular matrix to these mechanical events.

The extracellular matrix plays an important role in returning the whole muscle to its resting state. Although myofibroblasts in fascia have been shown to contract in a manner similar to smooth muscle (Schleip et al., 2006a,b), recovery from a highly stretched state may primarily involve a passive, elastic recoil of the extracellular matrix. Our light micrographs show that one key element—elastin—is distributed throughout the extensive extracellular matrix of the MIAA and at myotendon junctions (Fig. 22c,d,e). This element may provide enough elastic recoil to return whole muscle to its resting condition (Fig. 22f).

Our ultrastructural and histological results indicate that superstretched myofibrils are passively restored to their resting state by elastic recoil of superthin (titin) filaments (Fig. 21e), while a network of extracellular elastin contributes to restoring muscle fibres to their resting position within the whole muscle (Fig. 22f). During swallowing, the mandibles may separate even further than in the specimens we prepared for ultrastructural study. Unless sarcomeres stretch further, this would increase the discrepancy between overall muscle length and SL. SL upon immediate recovery is 18% shorter than SL_0, whereas muscle length is within 4% of initial length, suggesting that fibre and sarcomere recovery processes differ from whole-muscle recovery.

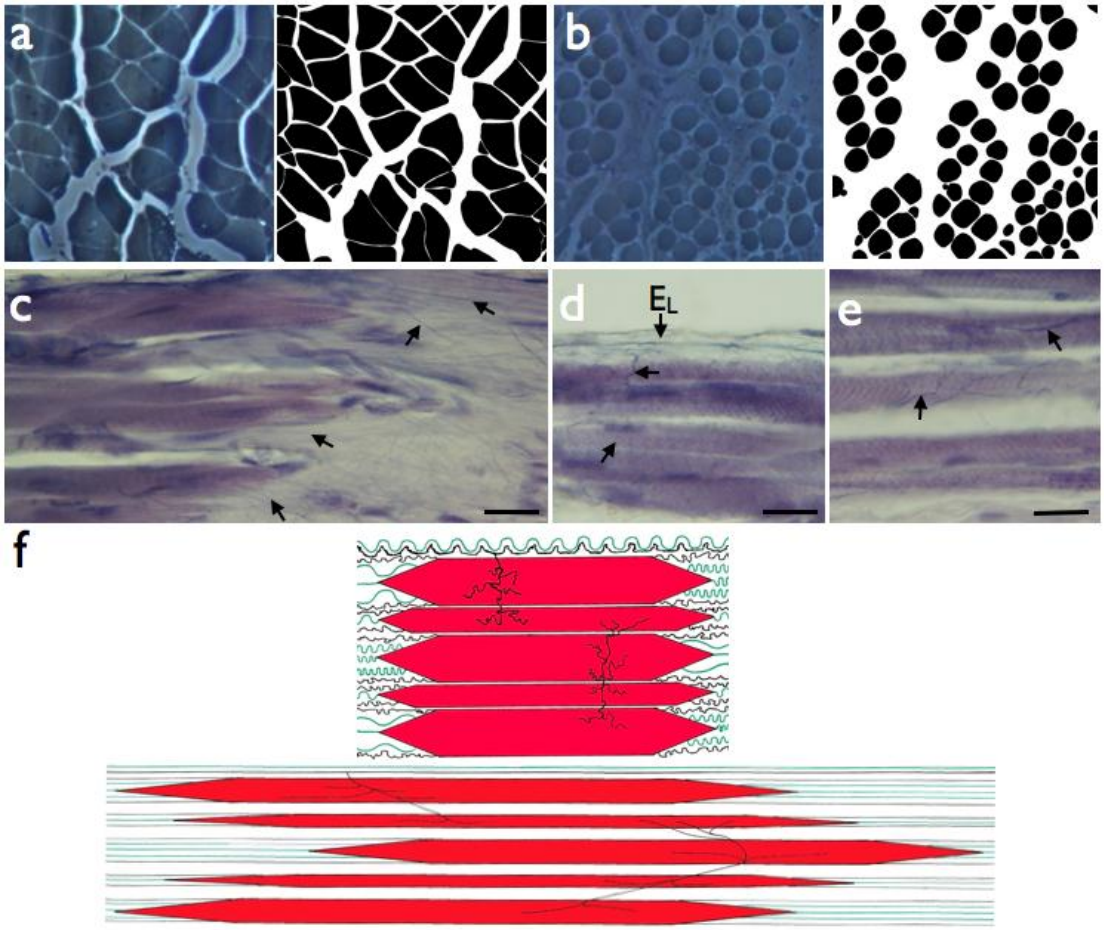
a
b
c
d
E_L
e
f

Figure 22. a–b) Light micrographs of cross-sections of resting (a) and stretched (c) muscle stained with toluidine blue and accompanying two-tone tracings illustrating the drastic change in muscle fibre shape and cross-sectional area upon extension. c–e) Light micrographs of moderately stretched muscle stained with iron gallein showing the distribution of elastin fibres (some of which are denoted by arrows) at the insertion site (c), anterior border of the muscle belly (d), and in the middle of the muscle belly (e). At the insertion, the muscle fibres are staggered in this moderately stretched condition, suggesting that fibres are able to move independent of one another depending on the length and extensibility of the myotendinous junction. Fine elastin filaments (barely detectible with the light microscope) radiate from the myotendinous junction into the raphe. At the anterior portion of the muscle belly, a lamina of elastin (E_L) can be seen along the convoluted collagenous epimysium, and this elastin filaments radiate inward and attach to the peri- and endo-mysia of adjacent fibres. Thick elastin fibres radiate from endo- and per-mysia between adjacent fibres and anchor to similar locations. Scale bars = 8μm. f) A two-dimensional model of whole muscle's passive stretching. Initially, collagen (green) and elastin (black) are highly convoluted in regions that will ultimately be displaced away from the origin and insertion during an extension event, but are less convoluted in regions that are tightly anchored. At the point beyond which individual fibres are maximally extended (~210% resting length), fibres begin to slip relative to one another as the intramuscular extracellular matrix begins to adjust relative to the plane of extension. At this point, collagen fibres become taught and possibly slip relative to one another, and elastin becomes highly extended. Recovery from this final state of extreme extension (>287% resting length) requires elastic recoil provided by the extended elastin.

Macrostomy is a feature of many snake taxa. Although the skeletal modifications that allowed for increased gape in snakes are well known, soft tissue properties are not. Our results show that the intermandibular muscles of snakes attain levels of extensibility that surpass the physiological limits of most vertebrate skeletal muscles, accomplished by modifications at cellular and subcellular levels.

METHODS SUMMARY

Northern watersnakes (*Nerodia sipedon)* were housed in the lab and fed fishes of sizes ranging from 20–90% of snake body mass. Feeding events were recorded and analysed for the degree to which the snake's mandibles separated during these events, and these distances were then used to determine the physiological limits by which to extend snake lower jaws in manual manipulations.

Three adult watersnakes were euthanised via decapitation following anesthesia. The lower jaws were removed and skinned, and each received one of three treatments: unstretched, stretched to 7X resting intermandibular distance, and stretched to 7X resting distance then allowed to recover. MIAA muscles from each specimen were fixed in position and subsequently prepared for transmission electron microscopy. TEM micrographs of Rest, Str, and Rec samples were collected and analysed for sarcomere length (SL), Z-line to A-band distance, Gap distance, distance between adjacent Z-lines (see Table 13), and relative position of triads.

Thick cross-sections of Rest and Str samples were collected and stained with toluidine blue in order to determine muscle fibre cross-sectional shape/ area differences between stretched and unstretched conditions. Longitudinal sections through an

additional watersnake lower jaw that had been moderately stretched was stained with iron gallein to determine the nature of the attachment site of the MIAA muscle fibres to its insertion and to determine presence and distribution of elastin in the extracellular matrix.

MATERIALS AND METHODS

Behavioural data during 164 normal feeding events were recorded with a Panasonic AG-456 camcorder for 10 adult and 15 juvenile and neonate *Nerodia sipedon*. Snakes were fed fish of masses scaled to premeasured intervals of snake mass. Fish maximum height and width was measured prior to feeding. These measures were later used to generate estimates of prey cross-sectional area which were combined with estimates of snake gape cross-sectional area provided measures of ingestion ratio (Prey cross-sectional area/ Snake gape). A subset of 49 feeding records for which the mass ratio was greater than 30% were then used to determine the limits to lower jaw extensibility. Video records included views of the lower jaw showing tips of the mandibles (intermandibular distance) at rest and at maximum gape during swallowing. We then used univariate general linear regression of ingestion ratio (x) on change in intermandibular distance (y) to determine the relationship between these two variables. Our behavioural records thus established the limits of extension of the intermandibular soft tissues, and these were subsequently used to establish limits and timing of our mechanical manipulations.

Experimental manipulations were carried out using three adult northern watersnakes of approximately the same size (average jaw length=28.3±2.0mm). Snakes were sacrificed via decapitation following anesthesia, and lower jaws of snakes were removed and then skinned in an isotonic snake ringer's solution. Exposed MIAA muscles

were kept wet with this solution during all experimental manipulations. Specimens were divided into three categories, Resting, Stretched, and Recovered. The lower jaw of the *Rest* specimen received no treatment. To stretch lower jaws of the Stretched and Recovered specimens, we first pinned the right mandible of each specimen to a dissecting tray and then sutured the left mandible to a wooden dowel held by a micromanipulator. Using the micromanipulator, we stretched lower jaws of both specimens a rate of 2 mm every 5 minutes until the desired degree of intermandibular extension was obtained (~700% resting intermandibular distance). The Stretched specimen was fixed at peak extension, but the mandible of the Recovered specimen was detached from the micromanipulator and the lower jaw was allowed to recover prior to fixing. Intermandibular distance and approximate muscle length for right and left MIAA muscles were measured prior to the stretch period, at peak extension, and following fixation using a miniscale or dial calipers. Following treatment, all specimens were fixed in an 8% Na cacodylate-buffered glutaraldehyde solution for 45 minutes prior to extraction of the muscles from the lower jaw. Finally, muscles were removed and stored in 4% glutaraldehyde.

For EM imaging, the tissue was post fixed in buffered 2% OsO_4 for 1 hr at 4^o C, en-bloc stained with uranyl acetate and embedded in epon. Thin sections were stained with lead citrate after cutting and examined in a Philips 410 electron microscope (Philips Electron Optics, Mahwah, NJ). The images were recorded digitally with a Hamamatsu C4742-95 digital camera (Advanced Microscopy Techniques, Chazy, NY). We measured intra-sarcomere distances using Fiji software, and interfibrillar Z-line distances were measured using Image J software (U.S. National Institutes of Health, Bethesda, MD, US).

Means were compared using Student's *t*-tests in Microsoft Excel (2010).

In order to determine whole muscle effects of stretching, thick cross-sections from Epon-embedded Resting and Stretched samples were cut and stained with toluidine blue. Images were then projected on a screen and muscle fibres were outlined, traced and shaded in order to improve contrast and reveal fibre shape/cross-sectional area of each condition. Finally, a paraffin-embedded, moderately stretched watersnake lower jaw was sectioned in transverse and longitudinal planes. In order to determine the occurrence and distribution of collagen and elastin in the endo-, peri- and epimysia of the MIAA, sections were subsequently stained with H&E and iron gallein elastin stain, mounted and viewed using compound light microscopy.

All methods were approved under Lehigh University IACUC Protocol 66.

Chapter 5

Epilogue

My observations of snakes feeding in the lab indicate that intermandibular distance (and thus distensibility of the lower jaw apparatus) can increase by more than 7X resting distance when prey of large mass ratios and ingestion ratios are consumed. The implications of highly extensible intermandibular soft tissues were pointed out by Cundall and Greene (2000) over a decade ago and have since been recognized in studies of watersnake feeding ecology (King, 2002), but, to date, only one other published study on feeding performance has shown intermandibular distance ("maximum displacement of mandibular tips"; Vincent et al., 2006b) to be positively correlated with prey size. Therefore, the work presented here explores the structural basis of a body region showing greater extensibility than most of those previously studied (Brainerd, 1994).

I initially intended to compare lower jaw distensibility in a number of snake species, two of which eat rodents. Early behavioral records for those species demonstrated that measuring prey size relative to snake gape size posed a number of problems poorly resolved in the previous literature (Loop and Bailey 1972; Shine 1991). This led to the approach I used in Chapter 2, where I used experimental manipulations of rodent prey to show that they are easily deformable into smaller shapes and sizes. I defined the ingestible size of rodent prey and quantified differences between ingestible size and standard measures of body size. My method provided a repeatable means to generate the measure of prey size thought to be most important to gape, cross-sectional area (Cundall and Greene 2000). Furthermore, it provided a means by which ingestible size—defined as the smallest attainable cross-sectional area of a prey item—could be

estimated from one or more single linear measures of body size. These observations on prey deformation make clear the complexity of analyzing feeding performance in gape-limited predators like snakes.

For snake ecologists, my methods offer a way to arrive at prey size from linear measures of conspecifics of rodent prey species found in stomach contents (Glaudas et al., 2008; Rodriguez-Robles, 1999a,b; Rodriguez-Robles, 2002). However, the method can and should be extended to other prey types. Because I assumed fish bodies were not deformable, I did not calculate ingestible sizes of fish prey used, but rather relied on measures of maximum cross-sectional area provided by others (King, 2002). Although the scaling relationships between linear measures of fish prey, circumferences, and diameters have been measured previously (Hailey and Davies, 1986), future work should address fish body deformability as well and focus on determining how measures scale to ingestible size.

In Chapters 3 and 4 I detailed an experimental approach to determining the structural basis of extreme extensibility in snake intermandibular soft tissues using the Northern watersnake (*Nerodia sipedon sipedon*). Though the importance of intermandibular soft tissue extensibility has been reiterated for decades (Gans, 1952; Arnold, 1983; Cundall and Greene, 2000), exactly how they stretch has remained elusive. The basic anatomical components of the system appear in wonderful descriptions, primarily in anatomical descriptions of the intermandibular muscles and hyolingual apparatus (Langebartel, 1968; McDowell, 1972; Groombridge, 1979; Cundall, 1995), but no evidence existed of what actually happened to these components when stretched.

Chapter 3 describes the changes accompanying high levels of extension in snake skin. Squamate skin is unique among vertebrates (Lange 1931; Maderson, 1964), and snakes represent a derived condition in which the basic elements (i.e., the partitioning of skin into rigid scale and flexible interscale regions) have been modified to maximize extensibility in the circumferential direction (Pockrandt, 1937; Savitzky et al, 2004; Rivera at al., 2005). Modifications for extreme skin extensibility exist in other vertebrates (Brainerd, 1994), but snakes possess two features that seem to be unique to the clade: an unusual, highly folded interscale skin and an elastic lamina supporting the dermis. My results indicate that as the skin is greatly extended during swallowing events, major folds of interscale skin flatten, the epithelium stretches, and the deep dermis stretches and thins. Elastin fibers anchored to the epidermis at the base of folds and to the elastic lamina stretch, and at the same time the lamina itself stretches in the plane of extension. My results suggest that the properties of elastin (Oxlund et al., 1988) allow passive recovery of the interscale skin to its unusual, highly folded state.

The changes seen in interscale skin in the highly stretched condition pose interesting questions relating to how cells of an epithelium change shape under high loads. In order for epithelial cells to stretch, there might be rearrangements of cell junctions at the basolateral surface to permit gross movement of the cell membrane and basal lamina.

The work in Chapter 4 addressed the following question: What happens to snake intermandibular muscles allowed to stretch and passively recover? I tested the hypothesis that snake intermandibular muscles would stretch to limits within the range seen during feeding (and beyond those of any vertebrate muscle studied) and would subsequently

recover in absence of direct stimulation. My results, gained through collaboration with Clara Franzini-Armstrong and Stefano Perni at the University of Pennsylvania, showed that at the cellular level, snake intermandibular muscles are highly extensible, extending to points beyond the limits of their ability to contract (i.e., beyond myofilament overlap), and yet recovering without contraction and without damage. Although high levels of extension have been applied to muscles and subsequent ultastructural changes documented (McNeil and Hoyle, 1967; Locker and Leet, 1975), no model accounts for the incredible degree of recoverable extension that we saw in snake muscle (210% resting distance for cells, 270% resting distance for whole muscle).

At the cellular level, snake lower jaw muscle stretches to limits that are within the known total length of vertebrate titin extension. However, the entire titin molecule is not extensible (Kellermayer et al. 1997; Linke et al. 1998) and given the variability of titin (Wang et al. 1993), it is possible that snakes possess a modified version of the molecule. Our results therefore lead us to hypothesize that titin in snake intermandibular muscles is long and is at least partly responsible for muscle recovery after regular degrees of extension beyond the muscle's physiological limits. What titin does not explain are gross deformations of the membrane components and interfibrillar architecture seen. For these, we suspect that other intermediate filaments play a key role (Pierobon-Bormioli, 1981; Tokuyasu et al., 1983; Wang et al., 1983). Research in the field of passive muscle extensibility should consider snake muscles as they recover from extreme levels of extension under normal physiological conditions in the living organism.

At the histological level, snake intermandibular muscles stretch to degrees that are higher than muscle fibers stretch (~270% vs. ~210% respectively), and therefore we

hypothesize that part of the mechanism of extension involves movement of fibers and/or varying attachments of fibers at myotendinous junctions. In either case, an elastic mechanism of recovery is necessary, and our histological data indicate that elastin may be abundant in the endo-, peri- and epimysial components of muscle. Other highly extensible muscles might reveal equally unusual intra- and extracellular modifications.

Chapters 3 and 4 detail ultrastructural and histological changes that accompany extension and recovery in two tissues from a single macrostomatan species. However, Macrostomata is among the most speciose clades of snakes (Greene, 1997) and the intermandibular soft tissues in members of this clade include more than skin and muscle (Young, 1998 a,b). Gross patterns in intermandibular muscle arrangement among snakes have been described by Groombridge (1979), and combined with the results of the present work on Northern watersnake muscles, they should shed some light on the types of adaptations that may have occurred to permit macrostomy. Given the major differences in anatomical arrangement between colubroids and booids (basal snakes), it is possible that cellular modifications are derived features of the clade. Similarly, though no synthesis of gross lower jaw scale patterns exists, preliminary observations suggest that there may be functional and evolutionary correlations to the size and arrangement of scales. Patterns in dorsal body scale row arrangement have been found (Savitzky et al., 2004), but to date the lower jaw scales have received little attention. Given the modifications of the anterior end of the snake for extensibility, and given snake skin's unique behavior, it is likely that the patterns have functional consequences.

In summary, most snakes are predators that ingest their prey whole. Throughout the evolution of snakes there has been a tendency for the feeding apparatus to increase in

size and mobility, allowing for increased gape. However, prey of large mass and ingestion ratios need not have fixed cross-sectional areas, and part of the success of macrostomatan snakes has to do with the deformability of prey that they exploit. The lower jaw apparatus also lacks a fixed cross-sectional area (as defined by skeletal properties), and the extensibility of soft tissues linking the mandibles depends on cellular and histological modification permitting time-dependent stretch. The timing of key ultrastructural and molecular events during extreme extension remains to be elucidated.

Bibliography

Alibardi L, Thomspon MB. 1999. Epidermal differentiation in the developing scales of embryos of the Australian scincid lizard *Lampropholis guichenoti*. J Morphol 241:139–152.

Alibardi L. 2002. Ultrastructure of the embryonic snake skin and putative role of histidine in the differentiation of the shedding complex. J Morphol 251:149–168.

Alibardi L, and Thompson MB. 2003. Epidermal differentiation during ontogeny and after hatching in the snake *Liasis fuscus* (Pythonidae, Serpentes, Reptilia), with emphasis on the formation of the shedding complex. J Morphol 256:29–41.

Arnold SJ. 1983. Morphology, performance and fitness. Am Zool 23:347–361.

Arnold SJ. 1993. Foraging theory and prey-size—predator-size relations in snakes. In: Seigel RA, Collins JT, editors. Snakes: Ecology and Behavior. New York: McGraw Hill Inc. pp 87–15.

Auen EL, Langebartel DA. 1977. The cranial nerves of the colubrid snakes *Elaphe* and *Thamnophis*. J Morphol 154:205–222.

Baden HP, Roth SI, Bonar LC. 1966. Fibrous proteins of snake scales. Nature Lond 212: 498.

Banerjee TK, Mittal AK. 1978. Histochemistry of the epidermis of the chequered water snake *Natrix piscator* (Colubridae, Squamata). J Zool Lond 185:415–435.

Banerjee TK, Mittal AK. 1980. Histochemistry of snake epidermis. In: Spearman, RIC and Riley PA, editors. The Skin of Vertebrates. London: Academic Press. pp 23–32.

Bauer A, Russell A, Shadwick R. 1989. Mechanical properties and morphological correlates of fragile skin in gekkonid lizards. J Exp Biol 145:79–102.

Bauer A, Russell A, Shadwick R. 1992. Skin mechanics and morphology in *Sphaerodactylus roosevelti* (Reptilia: Gekkonidae). Herpetologica 48:124–133.

Bauer A, Russell A, and Shadwick R. 1993. Skin mechanics and morphology of two species of *Pachydactylus* (Reptilia: Gekkonidae). S.-Afr Tydskr Dierk 28:192–197.

Berthé R, Westho VG, Bleckmann H, Gorb S. 2009. Surface structure and frictional properties of the skin of the Amazon tree boa *Corallus hortulanus* (Squamata, Boidae). J Comp Physiol A 195:311–318.

Borg, TK, Caulfield, JB. 1980. Morphology of connective tissue in skeletal muscle. Tissue Cell 12:197–207.

Brainerd EL. 1994. Pufferfish inflation: functional morphology of postcranial structures in *Diodon holocanthus*. J Morphol 220:243–261.

Brusca RC, Brusca GJ. 2003. Invertebrates, 2nd Ed. Sunderland, MA: Sinauer. 895 p.

Chiasson R, Lowe C. 1989. Ultrastructural scale patterns in *Nerodia* and *Thamnophis*. J Herpetol 23:109–118.

Chiasson R, Bently DL, Lowe C. 1989. Scale morphology in *Agkistrodon* and closely related crotaline genera. Herpetologica 45:430–438.

Churukian C, Schenk E. 1976. Iron gallein elastic method—a substitute for Verhoeff's elastic tissue stain. Stain Technol 51:213–217.

Clark RW. 2006. Fixed videography to study predation behavior of an ambush foraging snake, *Crotalus horridus*. Copeia 2006:181–187.

Craig A, Eikenberry E, Parry D. 1987. Ultrastructural organization of skin: classification on the basis of mechanical role. Connect Tissue Res 16:213–223.

Cundall D, Deufel A. 1999. Striking patterns in booid snakes. Copeia 1999:868–883.

Cundall D, Deufel A. 2006. Influence of the venom delivery system on intraoral prey transport in snakes. Zool Anz 245:193–210.

Cundall D, Greene HW. 2000. Feeding in snakes. In: Schwenk K, editor. Feeding: Form, Function and Evolution in Tetrapod Vertebrates. San Diego: Academic Press. pp 293–333.

Debelle L, Tamburro AM. 1999. Elastin: molecular description and function. Int J Biochem Cell Biol 31:261–272.

Dewsbury DA. 1992. Body mass and size in female deer mice, *Peromyscus maniculatus*, as a function of time since breeding. J Mammal 73:794–796.

Diefenbach CO, Emslie SG. 1971. Cues influencing the direction of prey ingestion of the Japanese snake, *Elaphe climacophora* (Colubridae, Serpentes). Herpetologica 27:461–466.

Dobson S. 1992. Body mass, structural size and life history patterns of the Colombian ground squirrel. Am Nat 140:109–125.

Dulhunty AF, Franzini-Armstrong C. 1975. The relative contributions of the folds and caveolae to the surface membrane of frog skeletal muscle fibers at different sarcomere lengths. J Physiol 250:513–539.

Fabien A, Bonnet X, Maumelat S, Bradshaw D, Schwaner T. 2004. Diet divergence, jaw size and scale counts in two neighboring populations of tiger snakes (*Notechis scutatus*). Amph-Rept 25:9–17.

Ficalbi E. 1888. Ricerche istologiche sul tegumento dei serpenti. Atti d. Soc. Toscana d. Sc. Nat., Pisa, 9, fasc. 1. (reviewed, in French, in Arch. Italienne de Biologie, 10:401–418.)

Forsman A, Lindell LE. 1993. The advantage of a big head: swallowing performance in adders, *Vipera berus*. Funct Ecol 7:183–189.

Frolich LM. 1997. The role of the skin in the origin of amniotes: permeability barrier, protective covering and mechanical support. Sumida S, Martin K, editors. Amniote Origins: Completing the Transition to Land. San Diego: Academic Press. pp 327–352.

Gans, C., 1952. The functional morphology of egg-eating adaptations in the snake genus *Dasypeltis*. Zoologica 37:209–243.

Gans C. 1961. The feeding mechanism of snakes and its possible evolution. Am Zool 1:217–227.

Gibson T, Kenedi RM. 1970. The structural components of the dermis and their mechanical characteristics. In: Montagna W, Bentley JP, Dobson, editors. Advances in biology of skin, vol. 10: The dermis. New York: Appleton-Century-Crofts. pp 19–38.

Glaudas X, Jezkova T, Rodríguez-Robles JA. 2008. Feeding ecology of the Great Basin Rattlesnake (*Crotalus lutosus*, Viperidae). Can J Zool 86:723–724.

Gower D. 2003. Scale microornamentation of uropeltid snakes. J Morphol 258:249–268.

Granzier HLM, Pollack GH. 1985. Stepwise shortening in unstimulated frog skeletal muscle fibers. J Physiol 362:173–188.

Greene H. 1983. Dietary correlates of the origin and radiation of snakes. Am Zool 23:431–441.

Greene HW. 1997. Snakes: The Evolution of Mystery in Nature. Berkeley:University of California Press. 366 p.

Hailey A, Davies PMC. 1986. Selection of prey from groups: watersnakes and fish. Herpetol J. 1:71–77.

Hampton PM. 2010. Morphology, Behavior, and Physiology of Feeding in Snakes. Dissertation, University of Louisiana at Lafayette. 123 p.

Hampton PM. 2011. Comparison of cranial form and function in association with diet in natricine snakes. J Morphol 272:1435–1443.

Herrel A, Meyers JJ, Timmermans JP, Nishikawa KC. 2002. Supercontracting muscle: producing tension over extreme muscle lengths. J Exp Biol 205:2167–2173.

Herrel A, Vincent SE, Alfaro ME, Van Wassenbergh S, Vanhooydonck B, Irschick DJ. 2008. Morphological convergence as a consequence of extreme functional demands: examples from the feeding system of natricine snakes. J Evol Biol 21:1438–1448.

Hogue A, Santos S.1953. Submicroscopic structure of "stratum corneum" of snakes. Science 118:410–411.

Horowitz R, Kempner ES, Bisher, ME, Podolsky RJ. 1986. A physiological role for titin and nebulin in skeletal muscle. Nature Lond 323:160–164.

Humason GL. 1979. Animal tissue techniques, 4th Ed. San Francisco: WH Freeman. pp 142–144.

Irish FJ, Williams EE, Seling E. 1988. Scanning electron microscopy of changes in epidermal structure occurring during the shedding cycle in squamate reptiles. J Morphol 197:105–126.

Iskjaer C, Slade N, Childs JE, Glass GE, and Korch GW. 1989. Body mass as a measure of body size in small mammals. J Mammal 70:662–667.

Jewell PA, Fullagar PJ. 1966. Body measurements of small mammals: sources of error and anatomical changes. J Zool Lond 150:501–509.

Jackson MK, Reno HW. 1975. Comparative skin structure of some fossorial and subfossorial leptotyphlopid and colubrid snakes. Herpetologica 31:350–359.

Jackson MK, Sharawy M. 1980. Scanning electron microscopy and distribution of specialized mechanoreceptors in the Texas rat snake *Elaphe obsoleta lindheimeri* (Baird and Girard). J Morphol 163:59–67.

Jayne B. 1988. Mechanical behaviour of snake skin. J Zool Lond 214:125–140.

Joseph P, Mathew J, Thomas V. 2007. Scale morphology, arrangement and micro-ornamentation in *Xenochrophis piscator* (Schneider), *Naja naja* (Linn), and *Eryx johni* (Russell). Zoo's Print Journal 22:2909–2912.

Kardong KV. 2012. Vertebrates: Comparative Anatomy, Function, Evolution, 6th Ed. New York, NY: McGraw-Hill. 794 p.

Kardong KV, Berkhoudt H. 1999. Rattlesnake hunting behavior: correlations between plasticity of predatory performance and neuroanatomy. Brain Behav Evol 53:20–28.

Kellermayer MSZ, Smith SB, Granzier HL, Bustamante C. 1997. Folding-unfolding transitions in single titin molecules characterized with laser tweezers. Science 276:1112–1116.

King RB. 2002. Predicted and observed maximum prey size – snake size allometry. Funct Ecol 16:766–772.

Klein M-CG, Deuschle JK, Gorb SN. 2010. Material properties of the skin of the Kenyan sand boa *Gongylophis colubrinus* (Squamata, Boidae). J Comp Physiol A 196:659–668.

Kley NJ, Brainerd EL. 2002. Post-cranial prey transport mechanisms in the black pinesnake, *Pituophis melanoleucus lodingi*: an x-ray videographic study. Zoology 105:153–164.

Kley NJ. 2006. Morphology of the lower jaw and suspensorium in the Texas blindsnake, *Leptotyphlops dulcis* (Scolecophidia:Leptotyphlopidae). J Morphol 267:494–515.

Landmann L. 1979. Keratin formation and barrier mechanisms in the epidermis of *Natrix natrix* (Reptilia, Serpentes): an ultrastructural study. J Morphol 162:93–126.

Lange B. 1931. Integument der Sauropsiden. In L. Bolk, E. Göppert, E. Kallius & W. Lubosch eds. Handbuch der vergleichenden Anatomie der Wirbeltiere, Band 1. Berlin: Urban & Schwarzenberg. pp 375–448.

Licht P, and Bennet A. 1972. A scaleless snake: tests of the role of reptilian scales in water loss and heat transfer. Copeia 1972:702–707.

Lillywhite H, and Maderson PFA. 1982. Skin structure and permability. In: Gans C, and Pough FH, editors. Biology of the Reptilia, Volume 12, Physiology C: Physiological Ecology. London: Academic Press. pp 397–442.

Locker RH, Leet NG. 1975. Histology of highly-stretched beef muscle: I. The fine structure of grossly stretched single fibers. J Ultrastr Res 52:64–75.

Loop MS, Bailey LG. 1972. The effect of relative prey size on the ingestion behaviour of rodent-eating snakes. Psychon Sci 28:167–169.

Maderson PFA. 1964. The skin of lizards and snakes. Brit J Herpet 3:151–154.

Maderson PFA. 1965a. Histological changes in the epidermis of snakes during the sloughing cycle. J Zool Lond 146:98–113.

Maderson PFA. 1965b. The embryonic development of the squamate integument. Acta Zool 46:275–295.

Maderson PFA. 1985. Some developmental problems of the reptilian integument. In: Gans C, Billett F, Maderson PFA, editors. Biology of the Reptilia, vol. 14B. New York: John Wiley & Sons. pp 525–598.

Magid A, Law DJ. 1985. Myofibrils bear most of the resting tension in frog skeletal muscle. Science 230:280–1282.

McArdle BH. 1987. The structural relationship: regression in biology. Can J Zool 66:2329–2339.

McNeil P, Hoyle G. 1967. Evidence for superthin filaments. Am Zool 7:483–498.

Mehta R. 2009. Early experience shapes the behavioral repertoires of hatchling snakes. J Ethol 27:143–151.

Mittal K, Singh N. 1987a. Scale epidermis of *Natrix piscator* during its sloughing cycle. Structural organization and protein histochemistry. J Zool Lond 213:545–568.

Mittal K, Singh N. 1987b. Hinge epidermis of *Natrix piscator* during its sloughing cycle. Structural organization and protein histochemistry. J Zool Lond 213:655–695.

Montagna W. 1962. The structure and function of skin. 2nd ed. Academic Press, New York. 454 p.

Montagna W, Bently JP, Dobson RL, editors. 1970. Advances in biology of skin, vol. 10: The dermis. New York: Appleton-Century-Crofts. 302 p.

Mori A. 1991. The effect of prey size and type on prey-handling behavior in *Elaphe quadrivittata.* J Herpetol 25:160–166.

Mori A, Vincent S. 2008. Determinants of feeding performance in free-ranging pit-vipers (Viperidae: *Ovophis okinavensis*): key roles for head size and body temperature. Biol J Linn Soc 93:53–62.

Moss M. 1972. The vertebrate dermis and the integumental skeleton. Am Zool 12:27–34.

Nagornyak E, Pollack GH. 2005. Connecting filament mechanics in the relaxed sarcomere. J Mus Res Cell Mot 26: 303–306.

Nishikawa KC. 1987. Staining amphibian peripheral nerves with Sudan Black B: progressive versus regressive methods. Copeia 1987:489–491.

Owings DH, Cross RG. 2008. Hunting California ground squirrels: constraints and opportunities for Northern Pacific Rattlesnakes. In: Hayes, WK, Beaman KR, Cardwell MD, Bush SP, editors. Biology of the Rattlesnakes. Loma Linda: Loma Linda University Press. pp 155–168.

Oxlund H, Manschot, J, Viidik A. 1988. The role of elastin in the mechanical properties of skin. J Biomech 21:213-–218.

Partridge SM. 1970. The biological role of cutaneous elastin. In: Montagna W, Bently J, Dobson, R, editors. The Dermis. New York: Meredith Corporation. pp 69–86.

Pockrandt D. 1937. Beitrage zur Histologie der Schlangenhaut. Zool Jb 62:275–322.

Pough FH, Groves JD. 1983. Specializations of the body form and food habits of snakes. Am Zool 23:443–454.

Price R. 1981. Analysis of the ecological and taxonomic correspondence of dorsal snake microdermatoglyphics. Ph.D. Dissertation, New York University, 164 p.

Price R. 1982. Dorsal scale microdermatoglyphics: ecological indicator or taxonomic tool. J Herpetol 16:294–306.

Queral-Regil A, King RB. 1998. Evidence for phenotypic plasticity in snake body size and head dimensions in response to amount and size of prey. Copeia 1998:423–429.

Pierobon-Bormioli S. 1981. Transverse sarcomere filamentous systems: 'Z- and M-cables'. J Mus Res Cell Mot. 2:401–413.

Pollack GH, Blyakhman FA, Liu X, Nagornyak E. 2005. Sarcomere dynamics, stepwise shortening and the nature of contraction. Adv Exp Med Biol 565:113–126.

Purslow PP. 1989. Strain-induced reorientation of an intramuscular connective tissue network: implications for passive muscle elasticity. J Biomech 22:221–312.

Rivera G, Savitzky AH, Hinkley JA. 2005. Mechanical properties of the integument of the common gartersnake, *Thamnophis sirtalis* (Serpentes: Colubridae). J Exp Biol 208:2913–2922.

Rodríguez-Robles JA. 2002. Feeding ecology of the North American gopher snakes (*Pituophis catenifer*, Colubridae). Biol J Linn Soc 77:165–183.

Rodríguez-Robles JA, Greene HW. 1999. Food habits of the long-nosed snake (*Rhinocheilus lecontei*), a 'specialist' predator? J Zool Lond 248:489–499.

Rodríguez-Robles JA, Bell CB, Greene HW. 1999a. Gape size and the evolution of diet in snakes: feeding ecology of erycine boas. J Zool Lond 248:49–58.

Rodríguez-Robles JA, Bell CB, Greene HW. 1999b. Food habits of the glossy snake, *Arizona elegans*, with comparisons of the diet of sympatric long-nosed snakes, *Rhinocheilus lecontei*. J Herpetol 33:87–92.

Roth SI, Jones WA. 1967. The ultrastructure and enzymatic activity of the boa constrictor (*Constrictor constrictor*) skin during the resting phase. J Ultrastr Res 18:304–323.

Roth SI, Jones WA. 1970. The ultrastructure of epidermal maturation in the skin of the boa constrictor. (*Constrictor constrictor*). J Ultrastr Res 32:69–93.

Rowe, RWD. 1981. Morphology of perimysial and endomysial connective tissue in skeletal muscle. Tissue Cell 13:681–690.

Salviati, G., Betto, R., Ceoldo, S. & Pierobon-Bormioli, S. 1990. Morphological and functional characterization of the endosarcomeric elastic filament. Am J Physiol. 259:144–149.

Savitzky A, Townsend V Jr, Hutchinson D, Mori A. 2004. Dermal characteristics, scale row organization, and the origin of macrostomy in snakes. J Morphol 260:325.

Schleip R, Naylor IL, Ursu D, Melzer W, Zorn A, Wilke HJ, Lehmann-Horn F, Klingler W. 2006. Passive muscle stiffness may be influenced by active contracitvity of intramuscular connective tissue. Med Hypoth 66:66–71.

Schleip R, Klingler W, Lehmann-Horn F. 2006. Fascia is able to contract in a smooth muscle-like manner and thereby influence musculoskeletal mechanics. Proceedings of the 5th World Congress of Biomechanics. Munich: Medimond pp 50–54.

Sherbrooke W, Scardino A. 2007. Functional morphology of scale hinges used to transport water: convergent drinking adaptations in desert lizards (*Moloch horridus* and *Phrynosoma cornutum*) Zoomorphol 126:89–102.

Shine R. 1991. Why do larger snakes eat larger prey items? Funct Ecol 5:493–502.

Shine R, Brown GP, Elphick MJ. 2004. Field experiments on foraging in free-ranging water snakes, *Enhydris polylepis* (Homalopsinae). Anim Behav 68:1313–1324.

Silva M. 1998. Allometric scaling of body length: elastic or geometric similarity in mammalian design. J Mammal 79:20–32.

Sokal R, Rohlf FJ. 1995. Biometry, 3rd edition. New York: W.H. Freeman. 880 p.

Swadżba E, Rupik W. 2010. A comparative studies of scales and gastrosteges formation in grass snake *Natrix natrix* L. (Lepidosauria, Serpentes) embryos. Acta Biol Crac Ser Bot 25:89.

Swadżba E, Rupik W. 2010. Ultrastructural studies of epidermis keratinization in grass snake embryos *Natrix natrix* L. (Lepidosauria, Serpentes) during late embryogenesis. Zoology 113:339–360.

Trombitas K, Greaser M, Labeit S, Jin J-P, Kellermayer M, Helmes M, Granzier H. 1998. Titin extensibility in situ: entropic elasticity of permanently folded and permanently unfolded molecular segments. J Cell Biol 140:853–859.

Tokuyasu KT, Dutton, AH, Singer, SJ. 1983. Immunoelectron microscopic studies of desmin (skeletin) localization and intermediate filament organization in chicken skeletal muscle. J Cell Biol. 96:1727–1735.

Vezina A. 1985. Empirical relationships between predator and prey size among terrestrial vertebrate predators. Oecologia 67:555–565.

Vincent SE, Herrel A, Irschick D. 2005. Comparisons of aquatic versus terrestrial predatory strikes in the pitviper, *Agkistrodon piscivorus*. J Exp Zool A Ecol Genet Physiol 303:476–488.

Vincent SE, Dang PD, Kley NJ, Herel A. 2006a. Morphological integration and adaptation in the snake feeding system: a comparative phylogenetic study. J Evol Biol 19:1545–1554.

Vincent SE, Moon BR, Shine R, Herrel A. 2006b. The functional meaning of "prey size" in water snakes (*Nerodia fasciata,* Colubridae). Oecologia 147:204–211.

Vincent SE, Moon BR, Herrel A, Kley N. 2007. Are ontogenetic shifts in diet linked to shifts in feeding mechanics? Scaling of the feeding apparatus in the banded watersnake, *Nerodia fasciata*. J Exp Biol 210:2057–2069.

Vincent SE, Brandley MC, Herrel A, Alfaro ME. 2009. Convergence in trophic morphology and feeding performance among piscivorous natricine snakes. J Evol Biol 22:1203–1211.

Wainwright S, Vosburgh F, Hebrank J. 1978. Shark skin: function in locomotion. Science 202:747–749.

Wang K, Ramirez-Mitchell RA. 1983. A network of transverse and longitudinal intermediate filaments is associated with sarcomeres of adult vertebrate skeletal muscle. J Cell Biol 96: 562–570.

Wang K, McCarter R, Wright J, Beverly J, Ramirez-Mitchell R. 1993. Viscoelasticity of the sarcomere matrix of skeletal muscles: the titin-myosin composite filament is a dual-stage molecular spring. Biophys J 64:1161–1177.

Weaver, RE. 2010. Chemosensory and behavioral ecology of the dipsadid snakes: *Contia tenuis*, *Diadophis punctatus*, and *Hypsiglena chlorophaea*. Dissertation, Washington State University. 137 p.

Young BA. 1998a. The comparative morphology of the intermandibular connective tissues in snakes (Reptilia: Squamata). Zool Anz 237:59–84.

Young BA. 1998b. The comparative morphology of the mandibular midline raphe in snakes (Reptilia: Squamata). Zool Anz 237:217–241.

Matthew T. Close

Curriculum Vitae

Department of Biological Sciences
111 Research Dr./ Iacocca Hall B217
Lehigh University
Bethlehem, PA 18015

Cell: (610) 428-7135
Lab: (610) 758-5807
Email: mtc205@lehigh.edu
www.lehigh.edu/~mtc205

EDUCATION

Doctor of Philosophy, Integrative Biology, September 2012
Title: Elements of Deformation and Stretching in Vertebrate Bodies
Lehigh University, Bethlehem, PA
Advisor: David Cundall, Ph.D.

Bachelor of Science, Biological Sciences, May 2003
Old Dominion University, Norfolk, VA

RESEARCH

Graduate Research, Lehigh University, August 2005-July 2012
Advisor: Dr. David Cundall

Research Assistant, Maryland Department of Natural Resources, Natural Heritage Program, April-October 2004
Principal Investigator: Scott A. Smith

TEACHING EXPERIENCE

Teaching assistant

Lehigh University (August 2005- May 2012)

- **Comparative Vertebrate Anatomy Laboratory** (4 semesters)
  Supervisor: Dr. David Cundall
- **Introduction to Cellular and Molecular Techniques Laboratory** (3 semesters)
  Supervisor: Dr. Margaret Kenna
- **Genetics Laboratory** (2 semesters)
  Supervisor: Dr. Margaret Kenna
- **Integrative and Comparative Biology** (4 semesters)
  Supervisors: Dr. David Cundall and Dr. Colin Saldanha

Instructor

Lehigh University (May-August 2006)

- **Biology for Non-Majors**
  Co-instructor: Dr. David Cundall

TEACHING EXPERIENCE (CONTINUED)

Summer School Biology Instructor

Oscar F. Smith High School, Chesapeake, VA (June-August 2003)

Substitute Teacher

Chesapeake Public Schools, Chesapeake, VA, (January 2003-April 2004)

PUBLICATIONS

Published

Grogan, W. and Close, M. 2008. *Cemophora coccinea copei* distribution record. *Herpetological Review* 39(3):370.

In Press

Close, M. and Cundall, D. Mammals as prey: estimating ingestible size. *Journal of Morphology*.

In Preparation

Close, M., Perni, S., Cundall, D. and Franzini-Armstrong, C. Intra- and intercellular mechanisms of extreme extensibility of snake *intermandibularis anterior* muscle.

Close, M. and Cundall, D. Snake lower jaw integument and its functional role in macrostomy.

Close, M. and Cundall, D. Lower jaw distensibility and feeding performance in snakes.

PRESENTATIONS

Contributed

Close, M. and Cundall, D. 2012. Mammals as snake prey: Determining ingestible size. Lehigh Valley Ecology and Evolution Symposium, DeSales University.

Perni, S., **Close, M.**, Franzini-Armstrong, C., Cundall, D. 2012. High levels of calsequestrin in some snake muscles. Why? Biophysical Society Annual Meeting, San Diego, CA.

Close, M. and Cundall, D. 2012. Extensible tissues and their contribution to macrostomy in snakes. SICB Annual Meeting, Charleston, SC.

PRESENTATIONS (CONTINUED)

Close, M. and Cundall, D. 2011. The snake lower jaw apparatus: arriving at a model for extreme extensibility. SICB Division of Vertebrate Morphology SE Regional Meeting, Wake ForestUniversity, Winston-Salem, NC.

Close, M. and Cundall, D. 2010. Differences in lower jaw form and function among three macrostomatan snake families. Joint Meeting of Ichthyologists and Herpetologists, Providence, RI.

Close, M. and Cundall, D. 2010. Prey size and its effect on snake lower jaw behavior. Lehigh Valley Ecology and Evolution Symposium, Lehigh University, Bethlehem, PA.

Close, M. 2009. Structure of the stretchy skin of the snake lower jaw. SICB Division of Vertebrate Morphology NE Regional Meeting, Brown University, Providence, RI.

Close, M. and Cundall, D. 2009. Anatomical and histological correlates to snake lower jaw function. Joint Meeting of Ichthyologists and Herpetologists, Portland, OR.

Close, M. and Cundall, D. 2008. Lower jaw extensibility in snakes. Lehigh Valley Ecology and Evolution Symposium, Lafayette College, Easton, PA.

Invited Seminars

Close, M. 2010. Snake lower jaw skin: the structure and function of an extremely extensible keratinized epithelium. Department of Biological Sciences Open House and Graduate Student Research Symposium, Lehigh University, Bethlehem, PA.

Undergraduate Mentee* Presentations

Tuttman, C.*, Cundall, D., Wise, T. and Close, M. 2012. Where does the snake esophagus begin? Lehigh Valley Ecology and Evolution Symposium, DeSales University, Bethlehem, PA.

Constantino, J.* and Close, M. 2009. *In vivo* mechanical behavior of snake intermandibular soft tissues. Department of Biological Sciences Undergraduate Research Symposium, Lehigh University, Bethlehem, PA.

AWARDS

Teaching Assistant of the Year (2012)
Lehigh University, College of Arts and Sciences
Teaching Assistant of the Year (2007)
Lehigh University, College of Arts and Sciences

AWARDS (CONTINUED)

Best Graduate Student Oral Presentation (2012)
Lehigh Valley Ecology and Evolution Symposium

Best Graduate Student Oral Presentation (2010)
Lehigh Valley Ecology and Evolution Symposium

FUNDING

Research Grants

- Herpetologists' League, Grant-In-Aid of Research, 2011 ($500)
- SigmaXi Scientific Research Society, Grant-In-Aid of Research, 2011 ($700)
- Forum Research Grant, Lehigh University, 2010 ($125)
- College of Arts and Sciences Graduate Research Grant, Lehigh University, 2008 ($700)

Travel Grants

- Graduate Student Senate Travel Award, Lehigh University, 2011 ($150)
- Graduate Student Senate Travel Award, Lehigh University, 2010 ($125)
- College of Arts and Sciences Travel Award, Lehigh University, 2009 ($400)
- Graduate Student Senate Travel Award, Lehigh University, 2009 ($175)

SERVICE

The Herpetologists' League
Co-President Graduate Student Committee, 2009-2012

Lehigh University
Biological Organization of Graduate Students, 2008-2012
Offices: Treasurer, Educational Support Officer
Graduate Student Dean's Advisory Council, 2007-2008, 2010-2011

Journal of Experimental Zoology Part A
Reviewer, 2008-present

PROFESSIONAL AFFILIATIONS

Sigma Xi Scientific Research Society, 2008-present
Society for Integrative and Comparative Biology, 2009-present
Herpetologists' League, 2009-present
La Mica Biological Station, 2011-present

REFERENCES

Dr. David Cundall, Professor
Department of Biological Sciences, Williams Hall Annex
Lehigh University, Bethlehem, PA 18015
Phone: (610) 758-3679
Email: dlc0@lehigh.edu

Dr. Alan H. Savitzky, Department Head
Department of Biology, Utah State University
5305 Old Main Hill, Logan, UT 84322
Phone: (435)-797-1909
Email: savitzky@usu.edu

Dr. Margaret A. Kenna, Manager of Instructional Labs
Department of Biological Sciences, 1 West Packer Avenue
Lehigh University, Bethlehem, PA 18015
Phone: (610) 758-3685
Email: makg@lehigh.edu

Scott A. Smith, Wildlife Ecologist
Maryland Department of Natural Resources
Wye Mills Field Office
909 Wye Mille Road, Wye Mills, MD 21679
Phone: (410) 827-8612
Email: sasmith@dnr.state.md.us